

1 Southern Ocean biological pump over the last glacial cycle from 2 new diatom transfer functions

3 Mathieu Rembauville¹, Sylvain Pichat^{1,2}

4 ¹Univ. Lyon, ENS de Lyon, Université Lyon 1, CNRS, UMR 5276 LGL-TPE, 69364, Lyon, France

5 ²Climate Geochemistry Department, Max Planck Institute for Chemistry, Mainz, Germany

6 *Correspondance to* : Mathieu Rembauville (mathieu.rembauville@ens-lyon.fr)

7 **Abstract.** We present new transfer functions to reconstruct deep ocean (~1000 m) particulate organic carbon (POC) flux
8 and particulate inorganic to organic carbon export ratio (PIC:POC) from diatom assemblage in the Southern Ocean. The
9 transfer functions were calibrated with modern sediment trap data covering the three ocean sectors of the Southern Ocean.
10 They were then applied to ten sediment cores located in the Antarctic Zone (AZ) in the three Southern Ocean basins. The
11 diatom community appears to **capture** efficiently the ecosystem structure that **govern** the **magnitude and stoichiometry of the**
12 **export fluxes POC flux and PIC:POC export ratio** with root mean square errors of the prediction ranging 17-19.6 %
13 depending on the transfer **function**. A consistent climatic signal is observed in all sediment cores : the reconstructed deep-
14 ocean POC export is higher during glacial than interglacial periods. The PIC:POC ratio is low during glacial periods and
15 increases quickly after glacial maxima. These two signals suggest that both the increase **in the magnitude of the** biological
16 carbon pump and the decrease in the carbonate counter-pump in the AZ during glacial periods could have contributed to the
17 decrease in atmospheric pCO₂. The reconstructed POC export is consistent **with nutrient utilization** derived from previously
18 published diatom-bound δ¹⁵N and total organic carbon content but differs from elemental Ba/Fe ratio, **hinting Ba potential**
19 **preservation issues in Southern Ocean sediments**. At the global Southern Ocean scale, the deep-ocean POC export flux
20 decreases by 50 % and the PIC:POC export ratio increases by 17 % during the last deglaciation. While the
21 glacial/interglacial POC flux change is comparable in the three SO sectors, the PIC:POC change is weaker in the Pacific,
22 suggesting a distinctive response of the calcifying plankton community to glacial conditions in this sector. We suggest two
23 mechanisms likely to increase the biological pump efficiency during glacial periods : 1) iron fertilization increasing primary
24 production combined with diatom spore formation that increases export efficiency, and 2) a northward extension of sea ice
25 edge supporting a greater zooplankton-mediated export that increases transfer efficiency. These new transfer functions
26 quantitatively support a glacial iron fertilization effect in the AZ, contrasting with the view of a fertilization effect restricted
27 to the Subantarctic Zone.

1 Introduction

The biological pump is defined as the vertical transfer of CO₂ from the mixed layer to the deep ocean through the production, export and partial remineralization of organic matter. The biological pump transfers carbon from superficial reservoirs associated with short residence time (atmosphere and mixed layer, residence time = years) to deep reservoirs associated with much longer residence time (deep ocean and sediments, residence time = thousand to millions years). The Southern Ocean (SO) is the largest ocean on Earth, connecting the three other oceanic basins and providing nutrients to the global ocean thermocline (Sarmiento et al., 2004). The majority of the modern SO waters are qualified as “high nutrient, low chlorophyll” (HNLC) due phytoplankton growth limitation by micronutrients such as iron (de Baar et al., 1990). The macronutrient excess and leakage to lower latitudes suggests that the biological pump ~~vertical transfer of particulate organic matter from the surface to the deep ocean, i.e. the biological pump,~~ is inefficient (Sarmiento and Toggweiler, 1984; Sigman et al., 2010). Ice cores revealed that during the Last Glacial Maximum (LGM, 19 000 – 23 000 years ago) atmospheric pCO₂ was ~90 ppmv lower than preindustrial levels (Petit et al., 1999). Physical processes have been invoked to explain the role of the SO in lowering LGM atmospheric pCO₂ such as changes in vertical stratification and dense water formation (Toggweiler, 1999; Sigman et al., 2010) or changes in sea-ice extent (Stephens and Keeling, 2000; Stein et al., 2020). However, these physical processes appear insufficient to explain the entire LGM pCO₂ decrease (Archer et al., 2000).

Another mechanism has been proposed to lower the atmospheric pCO₂ during glacial periods: an increased iron supply to the HNLC zones of the SO via increased atmospheric dust flux. The larger input of this essential and limiting micronutrient would have led to an increase in macronutrient utilization and a more efficient biological pump (Martin, 1990; Kohfeld et al., 2005; Jaccard et al., 2013; Martínez-García et al., 2014; Shoenfelt et al., 2018). Numerical models suggest that a stronger biological pump during the LGM could account for a 30 – 50 ppmv decrease in atmospheric pCO₂ (Bopp et al., 2003; Tagliabue et al., 2009; Lambert et al., 2015; Yamamoto et al., 2019). The first reconstruction of the biological pump during the LGM considered that the entire SO was fertilized, resulting in higher nutrient utilization and subsequent export production in both the Subantarctic Zone (SAZ) and the Antarctic Zone (AZ) south of the polar front (Moore et al., 2000). However, additional export proxies suggested a latitudinal response of the SO to glacial conditions : ~~an increased a~~ ~~more efficient~~ biological pump in the SAZ due to dust-driven fertilization of phytoplankton growth, but a ~~weaker less~~ ~~efficient~~ biological pump in the AZ due to higher stratification and lower micronutrient enrichment (François et al., 1997; Anderson et al., 2002; Kohfeld et al., 2005; Jaccard et al., 2013; Sigman et al., 2021). These results were established based on different production and/or export proxies applied to different latitudinal sectors of the SO.

An additional biological mechanism likely to affect atmospheric CO₂ is the carbonate counter-pump, i.e. the release of CO₂ associated with particulate inorganic carbon (PIC) precipitation by calcifying organisms (Frankignoulle et al., 1994). This CO₂ source lowers the effect of CO₂ sequestration into particulate organic carbon (POC) caused by the biological pump. Therefore, the PIC:POC ratio of the exported particles is an estimate of the carbonate counter-pump intensity (Sarmiento et al., 2002). An increased carbonate counter-pump was suggested during the last deglaciation in the SAZ of the SO Pacific sector (Duchamp-Alphonse et al., 2018) as well as during warm periods such as MIS 3 in the polar frontal zone (PFZ) of the Indian sector (Brandon et al., 2022) and MIS 11 in the SAZ of the Pacific sector (Anderson et al., 2024).

Several proxies have been proposed to reconstruct the biological pump in the past (Kohfeld et al., 2005). Organic carbon export has been derived from sediment organic carbon (Corg) concentration rate normalized to ²³⁰Th, i.e. ~~corrected~~

for sediment redistribution (Francois et al., 2004; Thöle et al., 2019) or from biological barite accumulation rate, ~~i.e. the true vertical biogenic barite flux~~, with biogenic barite or barium (Ba) excess defined as the difference between total Ba and Ba of lithogenic origin (Dymond et al., 1992; François et al., 1997; Hernandez-Sanchez et al., 2011). Nutrient utilization in the surface ocean has been estimated from stable isotopes such as $\delta^{15}\text{N}$ (Martínez-García et al., 2014; Studer et al., 2015, 2018; Wang et al., 2017) and $\delta^{13}\text{C}$ (Vollmer et al., 2022). Although these approaches provided key information on the relative changes in the biological pump during glacial/interglacial cycles or millennial events, they do not reconstruct absolute carbon fluxes. Quantitative estimates of the biological pump and carbonate counter-pump are needed to understand the impact of oceanic biological processes on the glacial/interglacial atmospheric CO_2 changes. Past oceanic conditions are commonly reconstructed quantitatively using transfer functions: a statistical relationship between oceanic variables and the community structure of a microfossil record (Juggins, 2013). The first transfer function was built to reconstruct past ocean temperature and salinity from pelagic foraminifer assemblage using factorial analysis followed by multiple linear regressions (Imbrie and Kipp, 1971). The modern analog technique was then proposed, calculating the foraminifer assemblage dissimilarity between down-core samples and a reference sample of known oceanographic conditions (Hutson, 1980). Both techniques were extended to siliceous microfossils to reconstruct glacial Southern Ocean temperature and sea ice extent (Gersonde et al., 2005), and further combined with chemical proxies to map the global ocean LGM temperature (Waelbroeck et al., 2009). More recently, partial least square regression (PLSR), was used to reconstruct past sea surface temperature from diatom assemblages in the North Atlantic (Berner et al., 2008) and the Southern Ocean (Esper and Gersonde, 2014).

Diatom are major contributors to the global ocean primary production (Field et al., 1998; Uitz et al., 2010) and might contribute up to 40 % of the global POC export from the surface ocean (Jin et al., 2006). Furthermore, the diatom community structure has a strong influence on the biological pump intensity and stoichiometry through species-species strategies such as resting spore formation and highly variable Si:C ratio (Tréguer et al., 2018). Sediment trap studies in the Southern Ocean have provided a quantitative link between diatom species and POC or biogenic silica fluxes (Salter et al., 2012; Rembauville et al., 2015; Rigual-Hernández et al., 2015a). In this study, we develop new transfer functions based on diatom community structure to reconstruct the deep-ocean (~1000 m) POC flux and PIC:POC export ratio. These transfer functions are calibrated on modern Southern Ocean sediment trap data and then applied to sediment cores in order to quantitatively reconstruct the variations in the intensity of the biological pump and the carbonate counter-pump over the last glacial cycle.

2 Materials and method

2.1 Sediment traps and sediment cores data

We compiled sediment trap records from the Southern Ocean (south of 40 °S) for which POC, PIC and diatom export fluxes were reported. We excluded 1) records in which only few diatom species were qualitatively or semi-quantitatively enumerated (e.g. Abelson and Gersonde, 1991; Fischer et al., 2002; Salter et al., 2012), 2) sediment traps located at less than 100 m above the seafloor as these are prone to sediment resuspension (e.g. Pudsey and King, 1997), and 3) upper ocean sediment traps deployed over shallow island plateaus as these are not representative of deep-ocean fluxes (Rembauville et

al., 2015). Eventually, the dataset contains 11 sediment trap locations from the SAZ to the seasonal ice zone (SIZ) in the Atlantic, Indian and Pacific sectors of the SO, at a mean depth of 1250 m (range 830 - 2000 m b.s.l.), with total collection duration from 321 to 2 328 days (Table 1, Fig. 1). These sediment trap data reflect the ecological and biogeochemical gradient from the SAZ to the SIZ. The dataset includes warm water species, ice-related species as well as bloom-forming species and covers a wide range of ~~biogeochemical fluxes magnitude and stoichiometry~~ POC flux and PIC:POC export ratio from iron-limited to naturally iron-fertilized sites (Fig. 2). All the traps are located above the calcite compensation depth of ~3000 to 4000 m in the Southern Ocean (Feely et al., 2004). The dataset represents a total number of 256 samples, however the samples distribution is not equal across the sediment trap locations (Table 1). In order to avoid a geographical bias in the transfer function due to the unequal sampling effort, seasonal averages of sediment trap data were calculated for spring (September to November), summer (December to February), autumn (March to May) and winter (June to August). Thereby each sediment trap location has the same weight in the transfer functions calibration. The deployment depths are located in the deep mesopelagic ocean where the PIC and POC flux attenuation with depth is low, most of the flux attenuation occurring in the upper mesopelagic ocean (Martin et al., 1987; Marsay et al., 2015). The depth-dependent POC and PIC flux attenuation factor is highly variable at short time and space scales (Marsay et al., 2015; Henson et al., 2023; Oetjens et al., 2025; Williams et al., 2025) and cannot be addressed individually for every location and season. For this reason, the biogeochemical fluxes were not normalized to a standard depth. ~~Although some sediment traps considered in the study are located in the upper circumpolar deep water (UCDW) that latter reaches the atmosphere at the Antarctic divergence, we consider the compiled fluxes as representative of the deep ocean (~1000 to 2000 m) where carbon can be sequestered over climate-relevant timescales from a few hundred years to millennia (Henson et al., 2012; Doney et al., 2024; Siegel et al., 2021).~~

To test and apply transfer functions, we also compiled Southern Ocean sediment cores records in which detailed diatom counts were previously published (Table 2). These are located in three of the four zones encompassed by the sediment traps (Fig. 1) and cover the last 15 ka to 150 ka. All the sediment core diatom data, the associated geochemical variables and the age models were accessed at www.pangea.de.

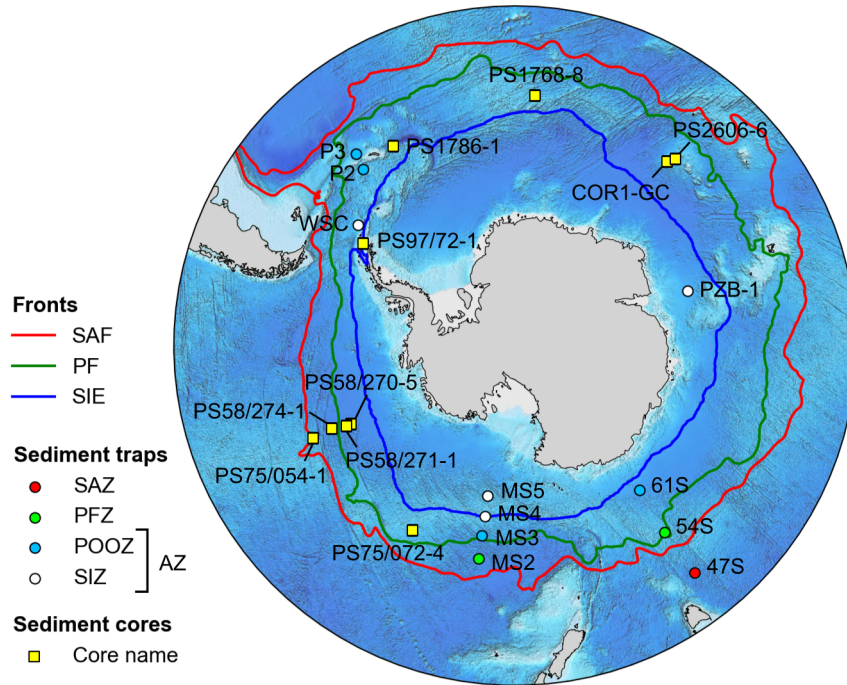


Figure 1. Location of the sediment traps (see Table 1 for details) and sediment cores (see Table 2 for details) used in this study. The subantarctic (SAF) and polar (PF) fronts are defined from dynamic topography (Park et al., 2019). Sea ice edge (SIE) refers to the September sea ice edge climatology (National Snow and Ice Data Center). SAZ: subantarctic zone, PFZ: polar frontal zone, POOZ: permanently open ocean zone, SIZ: seasonal ice zone, AZ: antarctic zone.

128 **Table 1.** Sediment trap records used to calibrate the diatom transfer functions. They are sorted along north-south transects
129 when existing. See Fig. 1 for locations.

Site	Zone	Lon. (°E)	Lat. (°N)	Depth (m)	Start date	Stop date	Duration (days)	Samples	Reference
MS-2	PFZ	-170,17	-56,9	982	1996-11-28	1998-01-27	425	20	Honjo et al., 2000; Grigorov et al., 2014
MS-3	POOZ	-170,05	-60,28	1003	1996-11-28	1998-01-27	425	12	Honjo et al., 2000; Grigorov et al., 2014
MS-4	SIZ	-169,9	-63,15	1031	1996-11-28	1998-01-27	425	13	Honjo et al., 2000; Grigorov et al., 2014
MS-5	SIZ	-169,67	-66,17	937	1996-11-28	1998-01-27	425	10	Honjo et al., 2000; Grigorov et al., 2014
47S	SAZ	142,07	-46,77	1060	1999-07-31	2001-10-13	805	29	Rigual-Hernández et al., 2015a
54S	PFZ	141,75	-53,75	830	1997-09-26	2004-02-10	2328	108	Rigual-Hernández et al., 2015b
61S	POOZ	139,9	-60,75	2000	2001-11-30	2002-09-29	303	20	Rigual-Hernández et al., 2015b
P2	POOZ	-41,12	-55,02	1500	2012-01-15	2012-12-01	321	9	Rembauville et al., 2016
P3	POOZ	-40,13	-52,72	2000	2012-01-15	2012-12-01	321	11	Rembauville et al., 2016
PZB-1	SIZ	72,98	-62,48	1400	1998-12-30	1999-12-13	348	13	Rigual-Hernández et al., 2019
WSC	SIZ	-53	-60	1000	2012-03-01	2013-02-01	337	11	Zúñiga et al., 2021

130 **Table 2.** Sediment cores used to apply the diatom transfer functions.

Core	Zone	Lon. (°E)	Lat. (°N)	Depth (m)	Diatom counts	Age model
PS97/72-1	SIZ	-56,06	-62,01	1993	Vorrath et al., 2023	Vorrath et al., 2023
PS1768-8	POOZ	4,48	-52,59	3270	Zielinski et al., 1998	Frank and Mackensen, 2002
PS1786-1	POOZ	-31,72	-54,92	5862	Jacot Des Combes et al., 2008	Jacot Des Combes et al., 2008
COR1-GC	POOZ	39,77	-54,27	2834	Orme et al., 2020	Orme et al., 2020
PS2606-6	POOZ	40,8	-53,23	2545	Jacot Des Combes et al., 2008	Jacot Des Combes et al., 2008 extended by Civel-Mazens et al., 2024
PS58/270-5	POOZ	-116,12	-62,03	4981	Benz et al., 2016	Benz et al., 2016
PS58/271-1	POOZ	-116,05	-61,24	5214	Esper and Gersonde, 2014	Benz et al., 2016
PS58/274-1	PFZ	-114,89	-59,21	5138	Benz et al., 2016	Benz et al., 2016
PS75/054-1	POOZ	-115,13	-56,15	4113	Benz et al., 2016	Benz et al., 2016
PS75/072-4	PFZ	-151,22	-57,56	3099	Benz et al., 2016	Benz et al., 2016

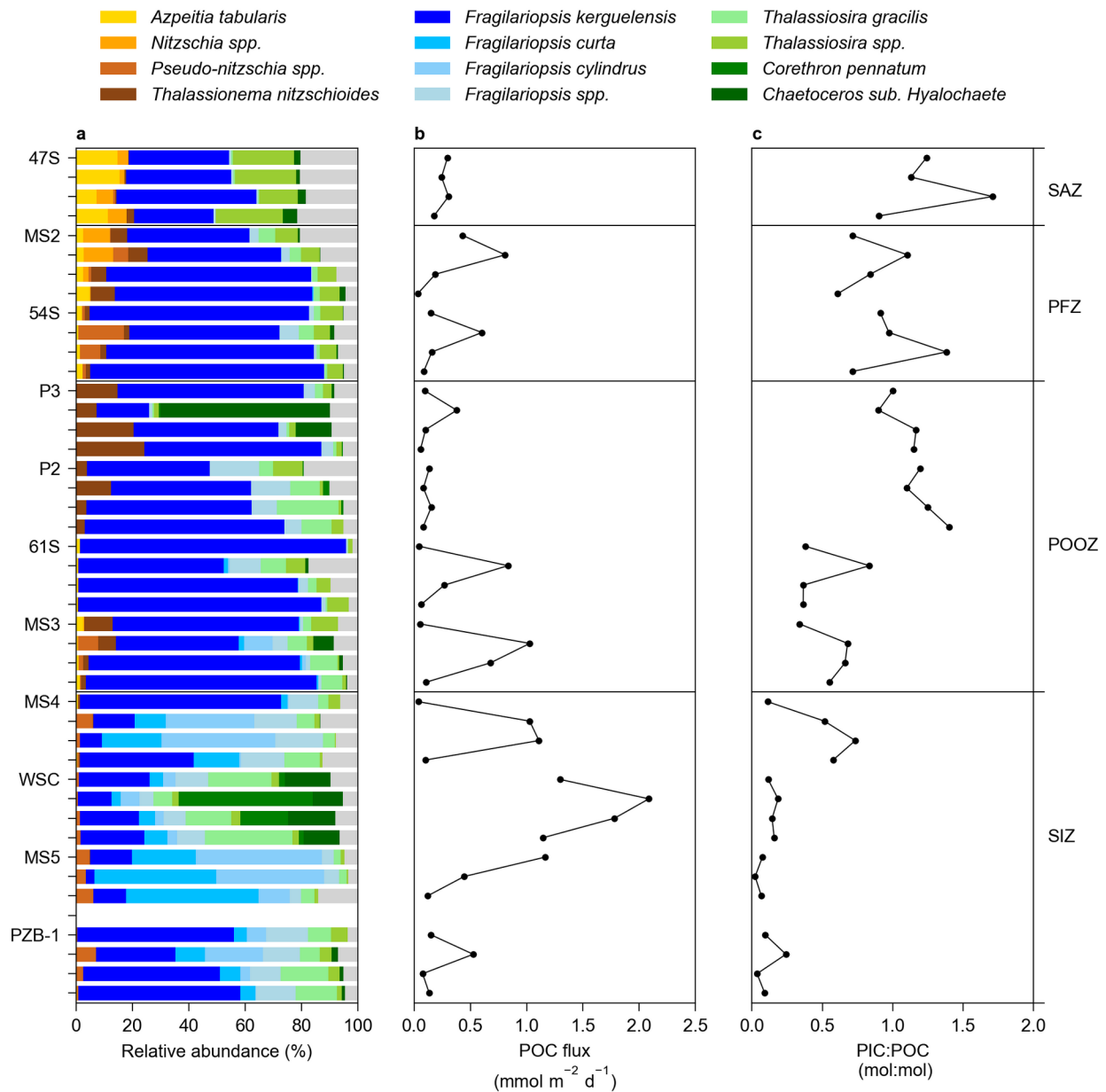
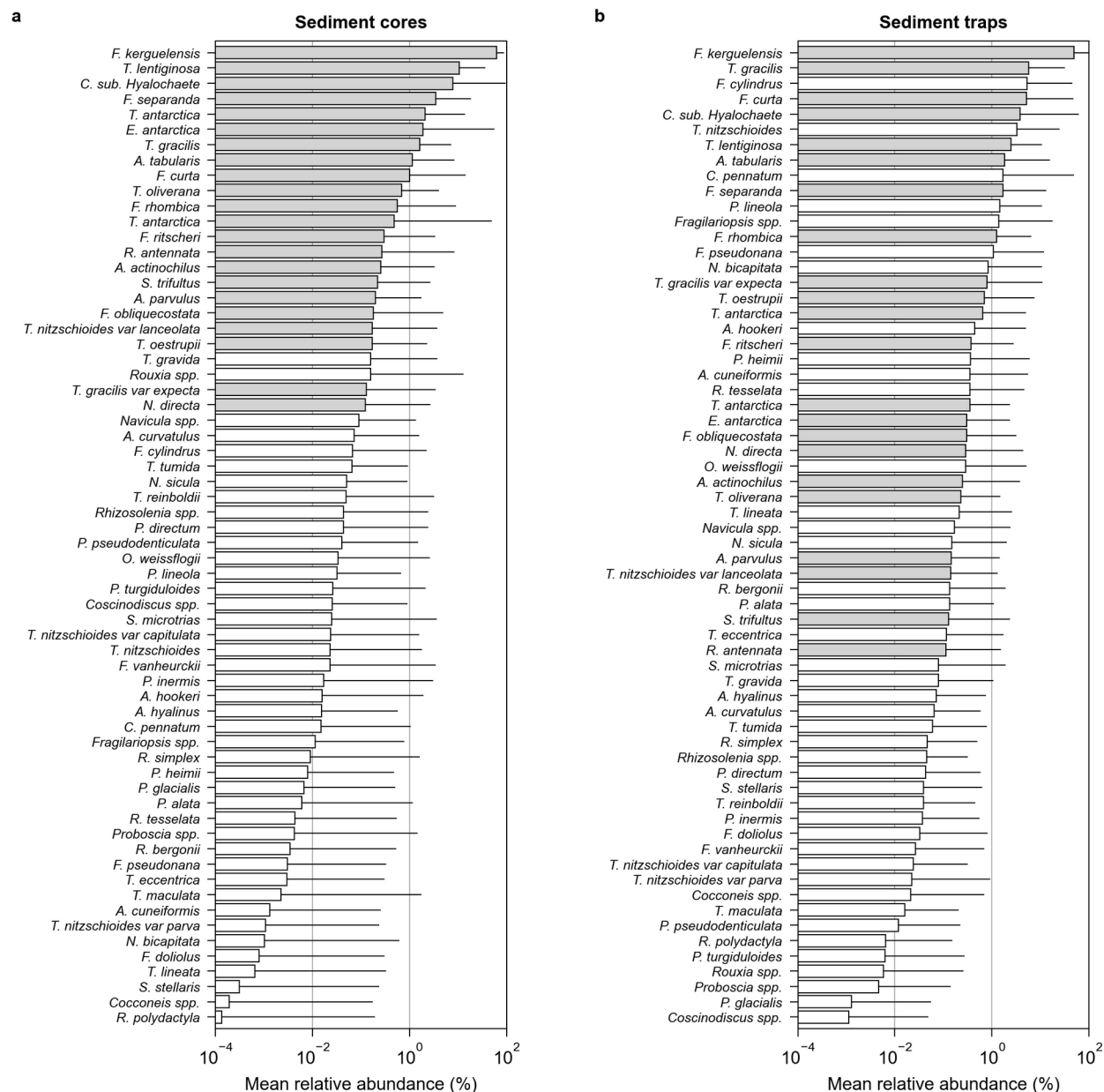


Figure 2. Seasonal averages of diatom species and biogeochemical fluxes from the sediment traps (see Fig. 1 and Table 1 for details). Sediment traps are sorted by location from north (top) to south (bottom) and for each sediment trap by season from spring (top) to winter (bottom). a) Relative abundance of the main diatom species (grey bars represent other species not reported in the legend). b) Particulate organic carbon (POC) flux. c) Particulate inorganic to organic carbon (PIC:POC) export ratio. Winter data are not available for trap MS5.

2.2 Diatom datasets homogenization

Diatom identifications reported in the sediment trap data are based on different sample preparation methods : some studies used a micropaleontological technique to oxidize organic matter (e.g. Grigorov et al., 2014; Rigual-Hernández et al., 2015) whereas others used a biological technique to differentiate full and empty frustules (Rembauville et al., 2016b). When the latter method was applied, the sum of empty and full frustule flux was used. The sediment trap data and the sediment core data contains 128 and 90 diatom species/taxa groups, respectively. Diatom species names were homogenized and updated to currently accepted taxonomic entities following Algeabase recommendations (www.algeabase.org) to a total number of 154 species/taxa group (see the Supplementary Information for the updated names and the full species list). As some sediment core records do not differentiate the vegetative stages from the resting spores (e.g. Jacot Des Combes et al., 2008; Orme et al., 2020), we chose to merge 1) *Chaetoceros* resting spores were with *Chaetoceros* subgenus *Hyalochaete* vegetative stages, 2) *Eucampia antarctica* resting spores with *Eucampia antarctica* vegetative stages and 3) *Thalassiosira antarctica* resting spores with *Thalassiosira antarctica* vegetative stages.

Our approach applies relationships between chemical fluxes and diatoms found in the mesopelagic/bathypelagic ocean (sediment traps) to sedimentary records. Indeed, the latter could potentially be affected by additional processes, e.g. diagenesis or sediment redistribution by deep-sea currents, that could modify the diatom community structure or the chemical fluxes. Diatoms are affected by selective grazing and dissolution during their sinking in the water column (Ran et al., 2024) and differential alteration of the frustule during early diagenesis (DeMaster et al., 1996; Pellegrino et al., 2024). For transfer functions calibration, the species present in both the sediment trap and sediment core datasets were first selected, i.e. 64 species/taxa groups (Fig. 3). Secondly, in order to avoid the bias associated with rare species and potential selective dissolution/preservation of species between the sediment trap and the surface sediments a filter was applied to isolate the abundant species shared by the two datasets. Species occurring with at least a relative abundance of 0.1 % in both datasets were selected (Esper and Gersonde, 2014). This final step resulted in a list of 22 informative species that we assume to be only marginally affected by dissolution and diagenesis, ensuring a robust transfer from the sediment trap to the sediment core datasets. The relative abundances of these informative species were rescaled to 100 % in the two datasets before using these data to calibrate the transfer functions.



161 **Figure 3.** Mean relative abundance of diatom species (bars) and highest relative abundance (lines) reported in a) the
 162 sediment core and b) the sediment trap datasets. Grey bars represent species with a mean relative abundance higher than 0.1
 163 % in both datasets.

2.3 Transfer functions development

Previous studies reported the direct quantitative link between plankton community structure and carbon export fluxes in sediment trap samples (e.g. Rembauville et al., 2015, 2016a, b). Such an approach needs a precise quantification of the full and empty diatom frustule flux together with the consideration of other flux vectors such as faecal pellets to estimate biovolumes and calculate carbon fluxes. The full/empty frustule distinction, the faecal pellets abundance, and the absolute fluxes are not available in sediment cores. Here, we use an alternative approach and suggest that the diatom community integrates the ecosystem structure that is the ultimate driver of the export fluxes. We do not formulate explicit mechanistic relationships between diatoms and POC or PIC fluxes. Rather, we consider that diatom community structure is correlated with biotic (e.g. other phytoplankton, zooplankton, calcifiers, bacteria) and abiotic conditions (hydrological zones, micronutrient availability) that altogether drive the biological pump and carbonate counter-pump. The seasonal sediment trap dataset was used to calibrate transfer functions in order to reconstruct the deep-ocean POC flux and PIC:POC export ratio based on the diatom diversity. Three transfer functions were built : multiple linear regression (MLR), partial least square regression (PLSR) and gradient boosting regression (GBR) using log-transformed and standardized diatom relative abundance (mean subtracted, divided by standard deviation).

For MLR, diatom relative abundances were transformed by factorial analysis with varimax rotation following the method developed by Imbrie and Kipp (1971). A scree test was used to identify significant factors associated with an eigenvalue > 1 (Cattell, 1966 ; Fig. S1), resulting in four informative factors used to build the linear model. While in the original method proposed by Imbrie and Kipp (1971), factors interactions and squared terms were added to the regression model, given the limited amount of data in our approach, we only used the linear combination of the four factors in order to avoid overfitting of multiple terms that artificially increases the model coefficient of determination (R^2) at the expense of higher error in the prediction from new data, i.e. the bias-variance tradeoff.

PLSR is a statistical method that builds a linear model between multivariate data by projecting the original matrices in a new space of maximum covariance. Dimensionality reduction restrains the weight of co-occurring species, making this approach useful to link ecological data with chemical fluxes (Rembauville et al., 2015, 2017; Salter, 2018; Blain et al., 2022). PLSR was already identified as an efficient method to build transfer functions from diatom assemblages in conjunction with MLR (Esper and Gersonde, 2014). The choice of the number of components to keep in the PLSR is another case of bias-variance tradeoff. To identify the significant components, the variance explained by the PLSR components was compared to a broken stick model, i.e. a null model in which decreasing variance is evenly distributed among components (Jackson, 1993). The first two components explained more variance than the null model and were thus selected for the PLSR calibration (Fig. S2).

GBR is a machine learning technique that builds a series of decision trees, each aimed at correcting the errors of the previous ones (Friedman, 2001). It produces a final model from an ensemble of weak predictive models. Each decision tree can integrate non-linear relationships and interactions that are not considered in linear modeling frameworks, making GBR a useful tool for the study of complex communities (Maloney et al., 2012). Two key parameters must be set when building a gradient boosting regressor : 1) tree depth, i.e. the number of nodes in the tree and 2) the number of estimators, i.e. the number of boosting stages that will be performed. These two parameters were selected using bootstrapping. The dataset was split into a learning set containing 2/3 of the data and a test set with the remaining 1/3 of the data. The root

mean squared error (RMSE) of the prediction was calculated for 10 000 permutations of train/test sets and performed with different combinations of tree depth and number of estimators. The combination minimizing the RMSE of the prediction for both the POC flux and the PIC:POC ratio was a tree depth of 2 with 30 estimators (Fig. S3).

The precisions of the MLR, PLSR and GBR transfer functions were calculated by bootstrapping using the same conditions as above (a learning set with 2/3 of the data, a test set with the remaining of the data, and 10 000 permutations).

2.4. Application of the transfer functions to sediment cores

The three transfer functions were applied to each of the sediment cores described in section 2.1 in order to quantitatively reconstruct the biological pump and carbonate counter-pumps over the last 15 to 150 ka in the various sectors of the Southern Ocean. Because sediment core samples integrate a pluriannual signal, the reconstructed POC fluxes were converted from seasonal to annual averages using a mean year duration of 365.25 days. All the data analyses were performed with Python and statistical models were implemented with the scikit-learn package (Pedregosa et al., 2011).

3 Results

3.1 Diatom species association with POC flux and PIC:POC ratio

The species scores on factors from the factor analysis used in the MLR prediction are presented in Table 3. Factor 1 is characterized by warm-water species typical of the SAZ (*Azpeitia tabularis*, *Shionodiscus trifultus*) and small *Thalassiosira* species such as *Thalassiosira oestrupii*, together with the giant mat-forming species *Thalassiothrix antarctica* often observed at the warm side of the fronts. Factor 2 is associated with ice-related species *Fragilariopsis curta* together with other small *Fragilariopsis* species displaying generally highest relative abundances in the SIZ (*F. separanda*, *F. rhombica*). Factor 3 contains bloom-forming and resting spore forming species generally observed in naturally iron-fertilized locations close to island systems and around the Antarctic coast (*Chaetoceros* subgenus *Hyalochaete*, *Eucampia antarctica*, *Thalassiosira antarctica*) together with less abundant species generally found in the POOZ (e.g. *Actinocyclus actinochilus*). Factor 4 contains rare and large species sometimes associated with the PFZ such as *Asteromphalus parvulus* and *Rhizosolenia antennata*. The MLR coefficients are provided in Table 4. The strongest positive correlation with POC flux is observed for factor 2 (ice-related species) and moderate positive correlations for factors 3 (spores and bloom-forming species) and 4 (large PFZ species). A negative correlation is observed for factor 1 (SAZ and warm-water species). For the PIC:POC ratio, a positive correlation is observed with factor 1 (SAZ warm-water species) whereas all the other factors are negatively correlated. The two MLR models for both POC flux and PIC:POC ratio are highly significant (global Fisher F-test, $p < 0.01$).

Species most positively correlated with POC export in the PLSR are *Actinocyclus actinochilus*, *Chaetoceros* subgenus *Hyalochaete*, *Fragilariopsis obliquecostata*, *Thalassiosira gracilis*, *Thalassiosira antarctica*, *Fragilariopsis rhombica*, and *Fragilariopsis curta* (Table 3, Fig. S4). All of them are positively associated with factors 2 (SIZ and ice-related species) and 3 (bloom-forming and spore-forming species). Species most positively associated with the PIC:POC

233 export ratio in the PLSR are *Thalassiosira oestrupii*, *Shionodiscus trifultus*, and *Azpeitia tabularis*. All of them are
 234 positively associated with factor 1 (SAZ species).

235 The most important species ($\geq 10\%$ in importance) in the GBR for POC flux are *Actinocyclus actinochilus*,
 236 *Chaetoceros* subgenus *Hyalochaete*, *Fragilariopsis kerguelensis*, *Fragilariopsis obliquecostata* and *Thalassiosira gracilis*
 237 (Table 5, Fig. S4). Most of them are positively associated with factor 3 (bloom-forming and spore-forming species). The
 238 most structuring species in the GBR for the PIC:POC export ratio are *Fragilariopsis curta* and *Fragilariopsis separanda*.
 239 Both species are positively associated with factor 2 (SIZ and ice-related species).

240 **Table 3.** Summary of transfer functions calibration : diatom scores on factors from the factor analysis (FA) with varimax
 241 rotation, partial correlation coefficients (β) from partial least square regression (PLSR), and features importance from
 242 gradient boosting regression (GBR). Major values are highlighted in bold.

Species	FA : scores on factors				PLSR : β coefficients		GBR : features importance (%)	
	F 1	F 2	F 3	F 4	POC	PIC:POC	POC	PIC:POC
<i>A. actinochilus</i>	-0.15	0.34	0.77	0.05	0.17	-0.06	29.8	0.0
<i>A. parvulus</i>	-0.19	0.03	-0.14	0.48	-0.09	-0.07	0.0	0.0
<i>A. tabularis</i>	0.94	-0.22	-0.15	-0.10	-0.02	0.08	0.3	1.8
<i>Chaetoceros</i> sub. <i>Hyalochaete</i>	0.13	-0.07	0.83	-0.05	0.15	0.03	12.3	1.1
<i>E. antarctica</i>	-0.39	-0.51	0.47	-0.18	0.04	0.07	0.1	0.2
<i>F. curta</i>	-0.22	0.81	0.14	0.17	0.07	-0.12	3.9	54.4
<i>F. kerguelensis</i>	0.09	-0.53	-0.37	0.02	-0.10	0.07	13.3	2.4
<i>F. obliquecostata</i>	-0.17	0.39	0.75	0.10	0.15	-0.07	16.9	6.3
<i>F. rhombica</i>	-0.13	0.58	0.38	0.53	0.10	-0.11	0.2	0.0
<i>Fragilariopsis ritscheri</i>	-0.07	0.71	-0.09	0.54	-0.01	-0.13	3.0	0.4
<i>F. separanda</i>	-0.20	0.63	0.06	0.27	0.06	-0.10	4.0	16.1
<i>N. directa</i>	-0.16	-0.52	0.00	0.17	0.01	0.07	0	0.2
<i>R. antennata</i>	0.12	0.04	0.01	0.63	-0.08	-0.04	3.1	0.4
<i>S. trifultus</i>	0.73	-0.05	0.06	-0.01	0.01	0.09	0.0	0.0
<i>T. nitzschioides</i> var <i>lanceolata</i>	0.31	-0.46	-0.04	0.15	-0.01	0.06	0.0	0.0
<i>T. antarctica</i>	-0.27	-0.05	0.79	-0.23	0.11	-0.01	1.5	0.2
<i>T. gracilis</i>	-0.44	0.51	0.20	-0.12	0.12	-0.03	9.0	1.8
<i>T. gracilis</i> var <i>expecta</i>	-0.05	0.08	0.02	0.99	-0.07	-0.08	0.0	4.8
<i>T. lentiginosa</i>	0.25	-0.12	-0.19	0.21	-0.01	0.04	0.8	0.1
<i>T. oestrupii</i>	0.88	-0.04	-0.12	-0.18	0.02	0.09	0.9	5.5
<i>T. oliverana</i>	0.10	-0.31	-0.28	0.34	-0.09	-0.05	0.0	4.3
<i>Tx. antarctica</i>	0.84	-0.09	-0.17	0.04	-0.04	0.06	0.7	0.0

243 **Table 4.** Coefficients of the multiple linear regression performed on the four factors from the factorial analysis of diatom
 244 relative abundance (log-transformed and standardized data). The last column contains the regression model *p*-value for each
 245 variable (F-test).

Response variable	Intercept	Factor 1	Factor 2	Factor 3	Factor 4	Model <i>p</i> -value
POC (mmol/m ² /d ⁻¹)	0.439	-0.136	0.330	0.046	0.066	4 .10 ⁻⁴
PIC:POC (mol:mol)	0.669	0.033	-0.149	-0.028	-0.224	2 .10 ⁻⁶

3.2 Transfer functions accuracy

Transfer functions coefficient of determination (R^2) varies depending on the method and the response variable considered (Fig. 4). The MLR, despite providing valuable information on the association of diatoms groups with export fluxes, has low R^2 values for both POC flux (0.41) and the PIC:POC ratio (0.56). The PLSR increases the prediction quality with R^2 reaching 0.68 for POC flux and 0.64 for the PIC:POC ratio. The GBR provided the highest R^2 for both the POC flux and the PIC:POC ratio (0.94 and 0.95, respectively). A better estimation of transfer function accuracy is provided by the calculation of the RMSE from bootstrapping (Fig. 5). For POC flux reconstruction, the highest mean error is associated with MLR (19.6 %), also characterized by a high error dispersion reaching up to 40 % while PLSR has the lowest mean error (17 %), associated with a low error dispersion. For the PIC:POC ratio, GBR has the lowest mean error (17.8 %) whereas MLR provides the lowest error dispersion.

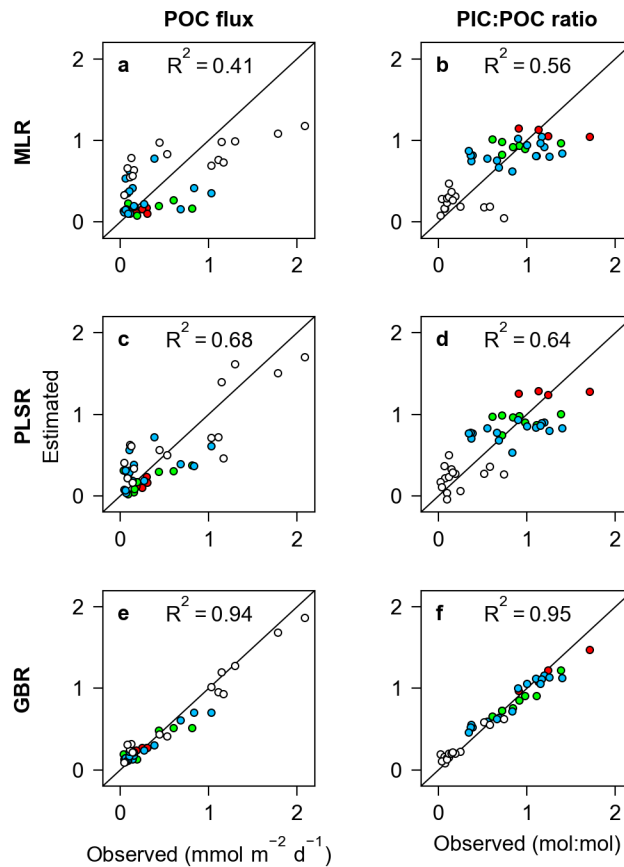


Figure 4. Biogeochemical fluxes (POC flux : particulate organic carbon flux, PIC:POC ratio: particulate inorganic to organic carbon ratio) estimated from the three transfer functions (MLR: multiple linear regression, PLSR: partial least squares regression, GBR: gradient boosting regression). Black line represents the 1:1 relationship, color code defines the four Southern Ocean zones as in Fig. 1.

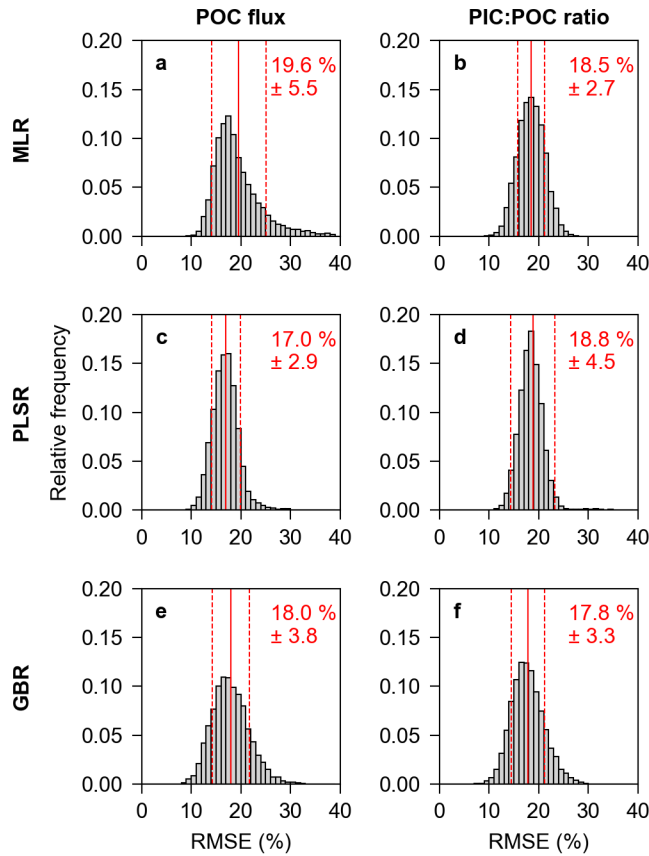
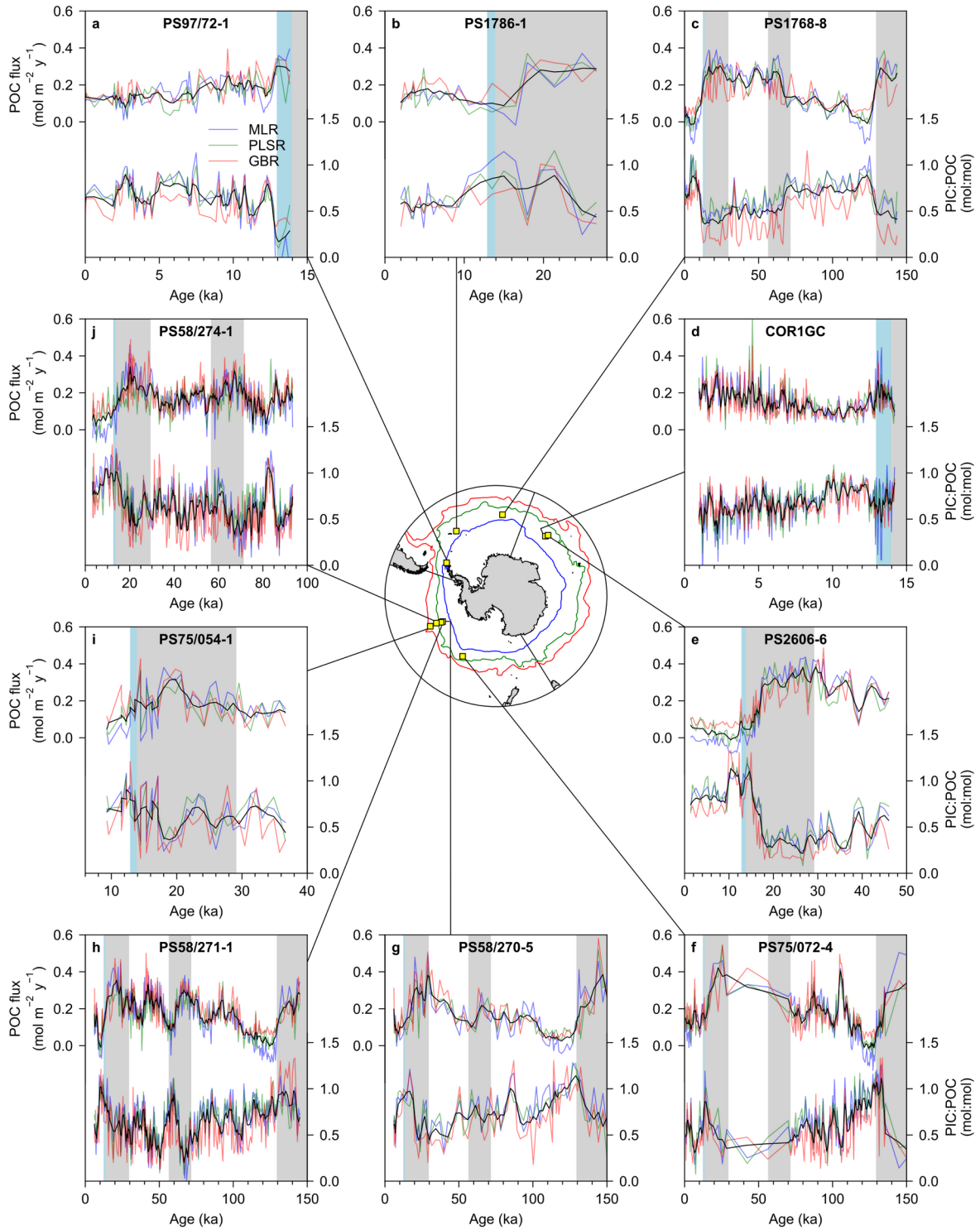


Figure 5. Root mean square error (RMSE) of the prediction for each transfer function and the two variables (POC flux and PIC:POC ratio) derived from bootstrapping (10 000 iterations). The red continuous and dotted lines show respectively the mean and one standard deviation around the mean.

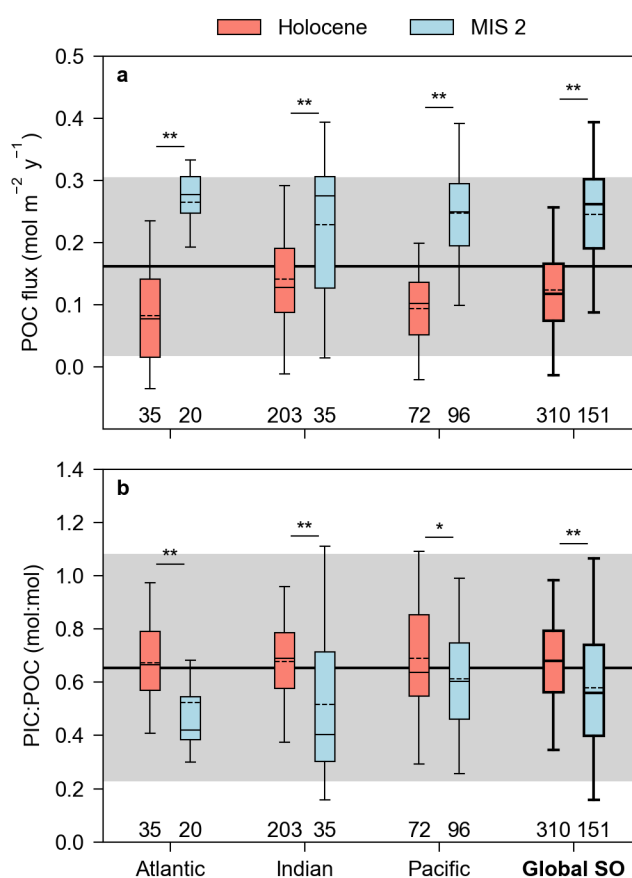
3.3 Reconstructed deep-ocean fluxes over the last glacial cycle

The three transfer functions provide convergent predictions with clear glacial/interglacial changes for the 10 sediment cores used in this study (Fig. 6). Reconstructed deep-ocean POC fluxes are higher during marine isotopic stages (MIS) 2, 4 and 6 associated with colder conditions and decrease during the Holocene and MIS 5 interglacials. An abrupt increase in PIC:POC ratio is observed during both deglaciations at the end of MIS 2 and MIS 6. These signals are observed in the three sectors of the Southern Ocean : Atlantic (Fig. 6b, c), Indian (Fig. 6e) and Pacific (Fig. 6f, g, h, i, j). The two cores with a high temporal resolution show similar trends during the Antarctic Cold Reversal (ACR) : a small increase in POC flux whereas the PIC:POC ratio slightly decreases (Fig. 6a, d). In the POOZ, throughout the Holocene, POC flux are lower at the beginning of the Holocene, followed by a gradual increase toward the modern area (Fig. 6b, c, d, e, g, h). This trend is not observed in the coastal SIZ where the POC flux remains low throughout the Holocene (Fig. 6a).



273 **Figure 6.** Application of the three transfer functions to sediment cores (blue: MLR - multiple linear regression, green: PLSR
 274 - partial least square regression, red: GBR - gradient boosting regression). Black lines represent the three transfer functions
 275 moving average. Vertical grey bars indicate marine isotopic stages (MIS) 2, 4 and 6. The vertical blue bar indicates the
 276 Antarctic Cold Reversal. Fronts represented in the central map are the same as in Fig. 1.

277 When focusing on the deep open-ocean, i.e. excluding the coastal SIZ core PS97/72-1, the three transfer functions
 278 show that the POC flux is significantly higher during MIS 2 compared to the Holocene in the three Southern Ocean basins
 279 (Fig. 7a). The MIS 2 mean global Southern Ocean POC flux is $0.25 \pm 0.09 \text{ mol m}^{-2} \text{ y}^{-1}$ (mean \pm standard deviation), ca. 1.5
 280 times the average modern mean sediment trap value, however remaining within the range of the observed modern values.
 281 Over the Holocene, the mean SO POC flux is $0.12 \pm 0.08 \text{ mol m}^{-2} \text{ y}^{-1}$ which represents 50 % of the MIS 2 flux. This
 282 Holocene mean value also overlaps with that of modern sediment trap fluxes. Changes in the PIC:POC export ratio appear
 283 more basin-specific (Fig. 7b). In the Atlantic and Indian sectors, the mean PIC:POC ratio increases from 0.52 to 0.68
 284 between MIS 2 and the Holocene whereas in the Pacific sector, the increase is only weakly significant from 0.61 to 0.68. In
 285 the three sectors, the reconstructed Holocene values are close to that of the modern sediment traps (0.65). The global
 286 Southern Ocean mean PIC:POC export ratio significantly increases from 0.58 to 0.68 (+17 %) from MIS 2 to the Holocene.
 287 The difference in the PIC:POC export ratio between MIS 2 and the modern sediment trap data is +13 %.



294 4 Discussion

295 4.1 Validity of diatom communities to reconstruct the ocean carbon pumps

296 The relative abundance of diatom species shows noticeable differences in the sediment trap and sediment core data. Small
297 ubiquitous species that are abundant in the sediment traps such as *Pseudo-nitzschia lineola* or *Nitzschia bicaudata* are rare
298 in the sediment cores. It is also the case for larger species such as *Corethron pennatum* and *Asteromphalus hookeri*. The
299 slope of the rarefaction curve is steeper in the sediment core dataset when compared to the sediment trap data, with the most
300 abundant species in the cores characterized by a heavily silicified frustule (e.g. *Fragilariopsis* and large *Thalassiosira*
301 species). These results confirm previous observations of selective dissolution of lightly silicified species in the deep ocean
302 below the sediment traps depth (Rigual-Hernández et al., 2016; Warnock and Krueger, 2020; Ran et al., 2024). Hence, the
303 selection of informative species in both datasets is a critical preliminary step before calibrating the transfer functions. The
304 resulting rather small number of informative species (here 22) is due to the merging of the sediment trap and sediment core
305 datasets in which the most abundant species are different. This number is however only slightly lower than those in studies
306 based on core-top diatom communities, typically 25 to 29 species (Imbrie and Kipp, 1971; Crosta et al., 1998; Esper and
307 Gersonde, 2014).

308 The convergence of the three transfer functions in every sediment core supports the reliability of the reconstructed
309 signals. The MLR is associated with higher error dispersion, potentially leading to negative values for periods of very low
310 POC flux. In this sense the PLSR and GBR appear as better estimators of POC export that are less prone to extrapolation
311 during periods of low or high flux. Globally the RMSE of the new transfer functions proposed here (17-19.6 %) is higher
312 than those of previously published diatom-based proxies: 5-6 % for summer the sea surface temperature (Esper and
313 Gersonde, 2014) and below 5 % for sea-ice cover (Crosta et al., 1998). The lower accuracy of the new proxies presented in
314 this study can be attributed to the restricted amount of sediment trap data available for the calibration (43 seasonal averages)
315 which is much lower than the abundant core-top data used in previously published diatom-based proxies (100 to 450
316 samples, Crosta et al., 1998; Esper and Gersonde, 2014). Despite this relatively high RMSE, the reconstructed POC flux and
317 PIC:POC ratio remain in the range of observed values in the SO modern ocean which supports the consistency of the
318 reconstructed values.

319 The factorial analysis clusters diatom species into ecologically consistent groups, highlighting hydrological zones
320 of the Southern Ocean as the most structuring factor of diatom biogeography as previously reported (Crosta et al., 1998;
321 Esper and Gersonde, 2014). Species associated with high scores on factors used in the MLR are consistent with the ones
322 that have both high partial correlation coefficients in the PLSR and a high importance in the GBR. This suggests that the
323 same ecological processes link the diatom community composition and the chemical fluxes in the three transfer functions,
324 resulting in comparable dynamics in the reconstructed variables. The deep-ocean POC flux is positively correlated with
325 bloom-forming and spore-forming diatoms from the POOZ and PFZ. An increase in the relative abundance of diatom
326 resting spore of *Chaetoceros* subgenus *Hyalochaete* and *Eucampia antarctica* during glacial periods was reported near the
327 continental shelf (Pesjak et al., 2023), close to island systems (Civel-Mazens et al., 2024), but also in the open water of the
328 SO (Abelmann et al., 2006; Jacot Des Combes et al., 2008). A direct quantitative link has already been established between
329 diatom resting spore vertical fluxes and POC export pulses downstream island plateaus where resting spore formation can
330 account for 40-60 % of the annual POC export (Salter et al., 2012; Rembauville et al., 2015, 2016b).

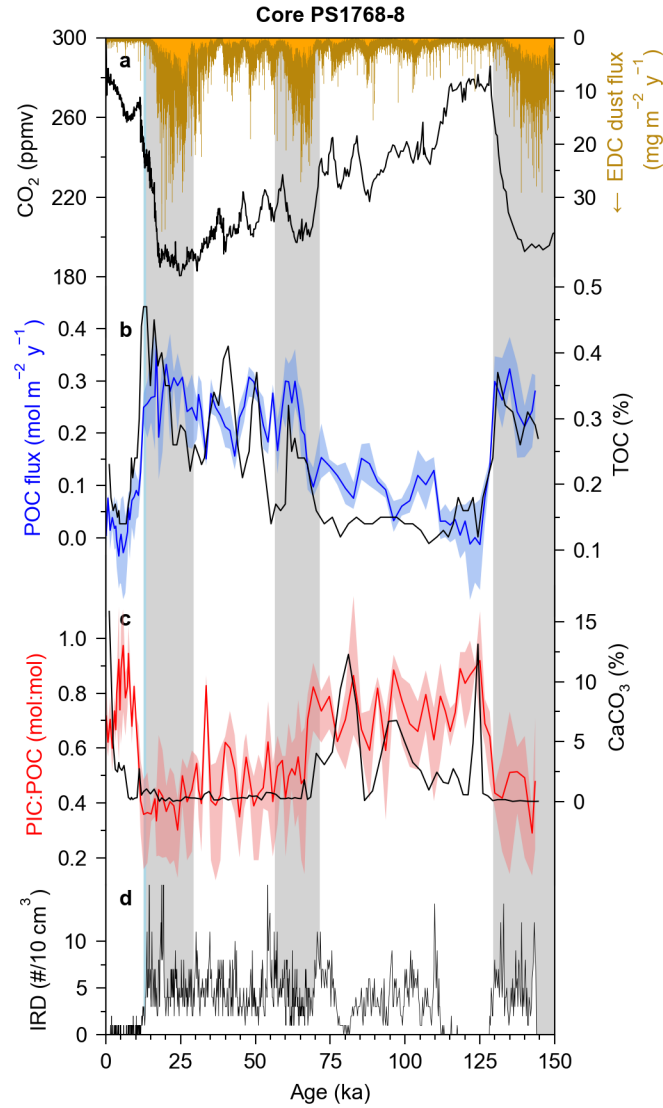
Cold water varieties of *Chaetoceros* subgenus *Hyalochaete* and *Eucampia antarctica* were reported to be associated with ice-related species such as *Fragilariopsis curta* and *F. cylindrus* in both modern and glacial sediment cores samples (Leventer, 1991; Armand et al., 2005; Abelmann et al., 2006). Here, the taxonomic resolution does not allow to differentiate the cold water varieties, but a similar co-occurrence is observed in the sediment core dataset (Fig. S6). The POC flux is positively correlated with SIZ and ice-related species of factor 2 (*Fragilariopsis curta*, *F. obliquecostata*). Copepod and krill feed on these ice-associated diatoms in summer (O'Brien et al., 2011; Schmidt et al., 2014; Pauli et al., 2021) and are efficient vectors of POC export through vertical migration and faecal pellet production (Smith et al., 2025). In this context, zooplankton-driven export can represent up to 90 % of the annual POC export in productive environments (Manno et al., 2015; Belcher et al., 2019). The efficient POC export by zooplankton feeding on ice-related diatoms could explain the association of SIZ and ice-related diatom with POC export in the transfer functions.

The PIC:POC ratio is positively correlated with warm water diatom species from the SAZ but negatively correlated with ice-associated diatoms. It has been previously reported that the PIC:POC export ratio increases north of the polar front concomitantly with an increase in the abundance of foraminifer and pteropod (Salter et al., 2014; Manno et al., 2022), whereas the PIC:POC export ratio is lower south of the polar front where the exported foraminifer flux decreases (Rembauville et al., 2016a). Although the calcifying plankton is not explicitly taken into account in this study, these results suggest that diatom communities, partially shaped by hydrological zones, appears to capture efficiently the global changes in ecosystem structure that set the magnitude of the carbonate counter-pump.

4.2 Local comparisons of the reconstructed fluxes with previously published data

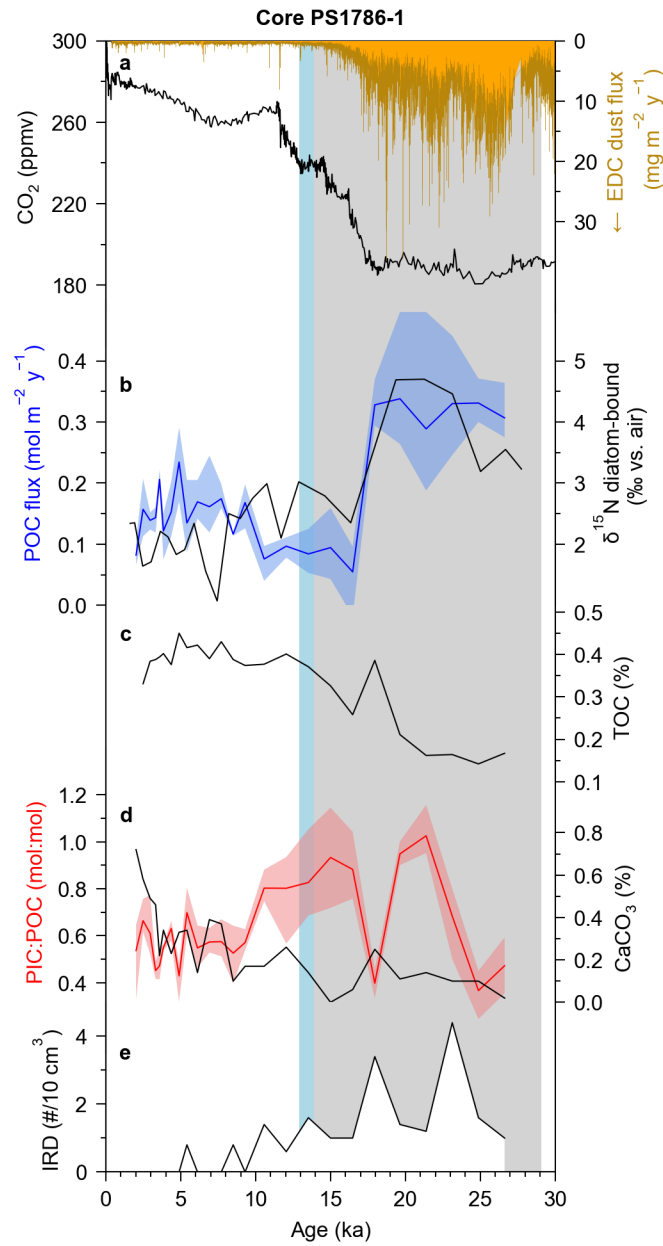
We compare the reconstructed POC flux and PIC:POC export ratio with previously published geochemical data for four sediment cores of the POOZ to estimate the validity of the reconstructed signals and identify potential mechanisms likely to explain the observed glacial/interglacial changes.

In core PS1768-8 (Atlantic sector), periods of high POC fluxes match increases in dust flux and decreases in atmospheric CO₂ (Fig. 8a). The POC flux variations coincides with that of the total organic carbon (TOC) content (Fig. 8b) and shows high values associated with high IRD abundance during MIS 2 and MIS 6 (Fig. 8d). Peaks in PIC:POC ratio and CaCO₃ content occur in the absence of IRD during the Holocene and during MIS 5 at 80 ka and 120 ka. The reconstructed PIC:POC export ratio is globally correlated with the CaCO₃ content, with higher values during interglacials and lower values during cold periods (Fig 8c).



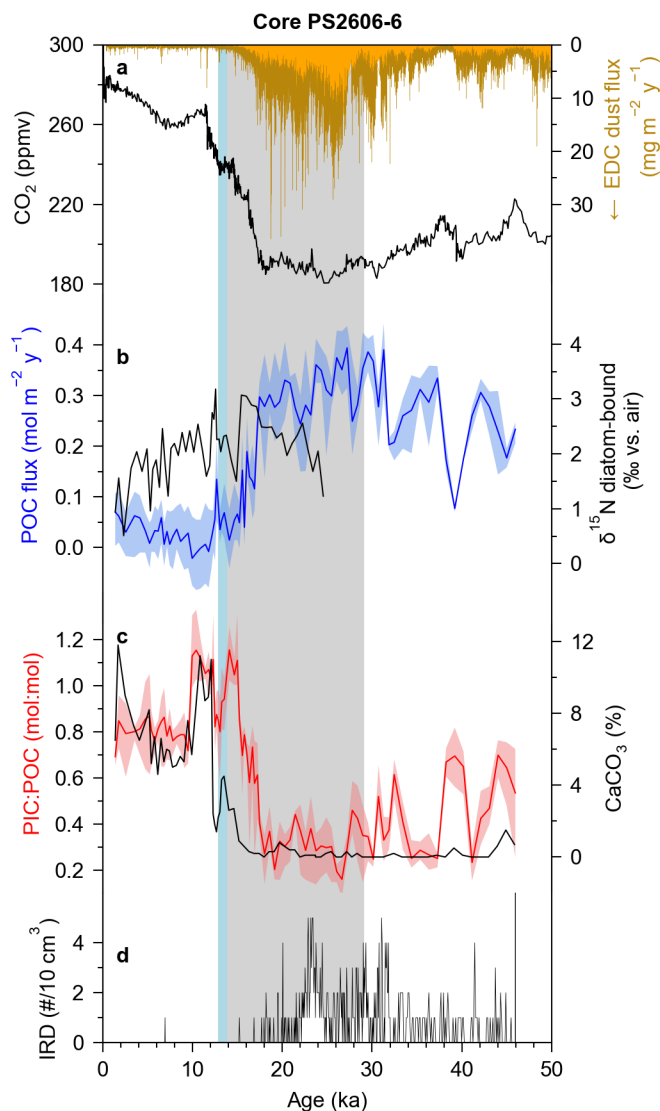
358 **Figure 8.** Comparison of the reconstructed POC export flux and PIC:POC ratio with previously published data for core
 359 PS1768-8. a) Atmospheric CO₂ (black, Bereiter et al., 2015) and dust flux (brown, Lambert et al., 2012) from EPICA Dome C
 360 (EDC) ice core. b) Reconstructed deep-ocean POC flux (blue, this study) and sediment total organic carbon (TOC) content
 361 (black, Kuhn and Bohrmann, 1996). c) Reconstructed PIC:POC export ratio (red, this study) and sediment CaCO₃ content
 362 (black, Kuhn and Bohrmann, 1996). d) Ice rafted debris (IRD) abundance (Diekmann et al., 1996). In b) and c), the
 363 continuous line is the transfer functions average and the colored area is the transfer functions envelope. Grey and blue bars
 364 as in Fig. 6.

365 In core PS1786-1 (Atlantic sector), the highest POC flux of $0.3 \text{ mol m}^{-2} \text{ d}^{-1}$ during the LGM is concomitant high
366 dust flux, low atmospheric CO_2 (Fig. 9a) and high diatom-bound $\delta^{15}\text{N}$ values (Fig. 9b). The large POC flux and diatom-
367 bound $\delta^{15}\text{N}$ decreases between ca. 18 and 15 ka are concomitant. However, during the late Holocene the two signals are not
368 correlated. The reconstructed POC flux is correlated with the TOC content during the Holocene and deglacial but not during
369 the glacial maxima. Contrary to core PS1768-8 (Fig. 8), the reconstructed PIC:POC export ratio is not correlated with the
370 CaCO_3 content (Fig. 9c). Decreases in the PIC:POC export ratio are associated with increases in the abundance of IRD
371 during MIS 2. For this core, both the TOC and CaCO_3 content must be taken with caution due to 1) potential dilution effects
372 by variable abundance of detrital sediments, especially during the last glacial and 2) the core depth (5862 m b.s.l.) which is
373 deeper than the carbonate compensation depth, that can result in important CaCO_3 dissolution. Both processes could
374 contribute to the low TOC and CaCO_3 contents observed in this core and partly explain their temporal variations.



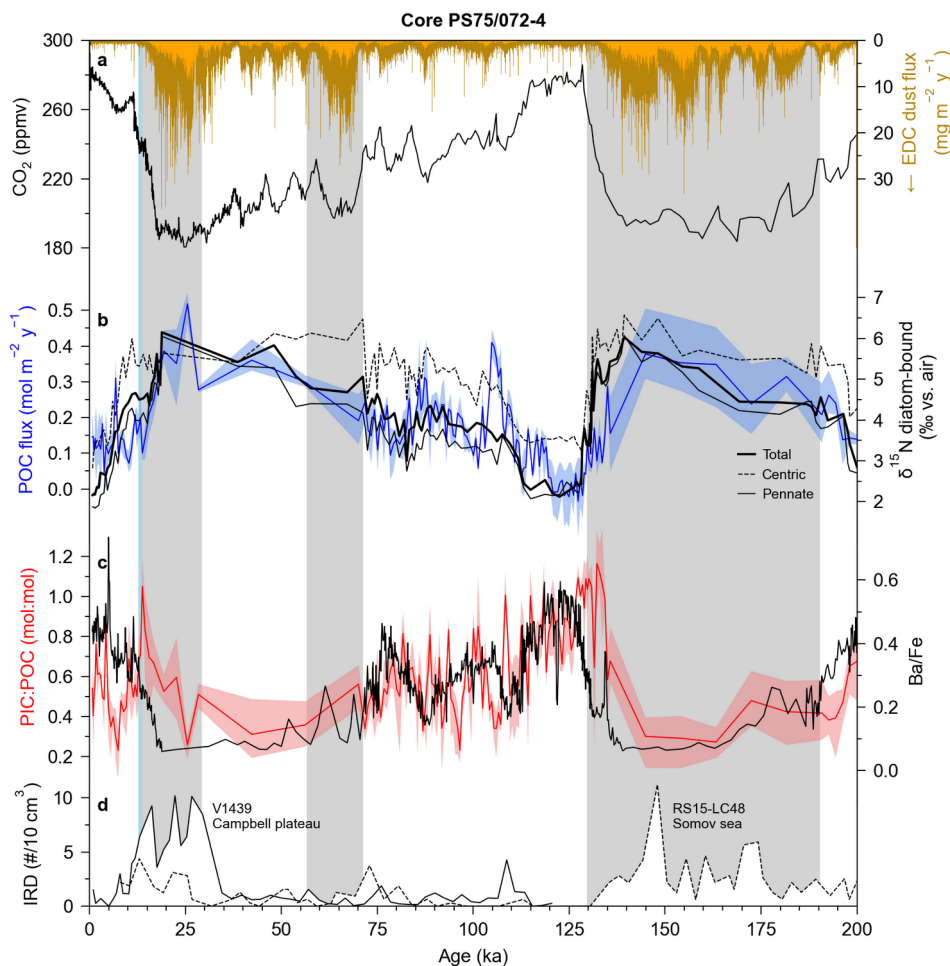
375 **Figure 9.** Comparison of the reconstructed POC flux and PIC:POC ratio with previously published data for core PS1786-1.
 376 a) Atmospheric CO₂ (black, Bereiter et al., 2015) and dust flux (brown, Lambert et al., 2012) from EPICA Dome C (EDC)
 377 ice core. b) Reconstructed deep-ocean POC flux (blue, this study) and diatom-bound δ¹⁵N (black, Jacot Des Combes et al.,
 378 2008). c) **Total organic carbon (TOC) content (Grobe, 1996).** d) Reconstructed PIC:POC export ratio (red, this study) and
 379 sediment core CaCO₃ content (black, Grobe, 1996). e) Ice rafted debris (IRD) abundance (Grobe, 1996). In b) and c), the
 380 continuous line is the transfer functions average and the colored area is the transfer functions envelope. Grey and blue bars
 381 as in Fig. 6.

382 In core PS2606-6 (Indian sector), the highest POC flux ($0.3\text{--}0.4 \text{ mol m}^{-2} \text{ y}^{-1}$) is again concomitant with high dust
 383 and low atmospheric CO_2 during MIS 2 but is not correlated with the low diatom-bound $\delta^{15}\text{N}$ values ($1\text{--}2 \text{ ‰}$) between ca. 25
 384 ka and 18 ka (Fig. 10a, b). However, both records seem to co-evolve around the ACR from ca. 18 ka to 10 ka. The PIC:POC
 385 ratio increases from 0.3 to 1 between the LGM and the beginning of the Holocene which is matched by the abrupt increase
 386 in the CaCO_3 content from 0 to 12 % between 18 ka and 12 ka (Fig. 10c).



387 **Figure 10.** Comparison of the reconstructed POC export flux and PIC:POC ratio with previously published data for core
 388 PS2606-6. a) Atmospheric CO_2 (black, Bereiter et al., 2015) and dust flux (brown, Lambert et al., 2012) from EPICA Dome
 389 C (EDC) ice core. b) Reconstructed deep-ocean POC flux (this study) and diatom-bound $\delta^{15}\text{N}$ (Jacot Des Combes et al.,
 390 2008). c) Reconstructed PIC:POC export ratio (this study) and sediment core CaCO_3 content (Kuhn, 2003). d) Ice rafted
 391 debris (IRD) abundance (Grobe, 2001). In b) and c), the continuous line is the transfer functions average and the colored
 392 area is the transfer functions envelope. Grey and blue bars as in Fig. 6.

393 In core PS75/72-4 (Pacific sector), high POC fluxes are again concomitant with high dust fluxes and high IRD
 394 abundance during MIS 2 and MIS 6 (IRD are not quantified in core PS75/072-4, data comes from two cores RS15-LC48
 395 and V1439 located in the southern and northern parts of the Pacific sector, respectively). The MIS 5 shows short events of
 396 increased POC flux associated with increased dust fluxes at 80-85 ka and 105-110 ka (Fig. 11a, b). The POC flux closely
 397 matches the diatom-bound $\delta^{15}\text{N}$ although the correlation is less evident when considering only the centric diatoms (Fig.
 398 11b). The PIC:POC export ratio is higher at the beginning of MIS 5 and decreases during MIS 2-4 and MIS 6 (Fig. 11c).
 399 The Ba/Fe ratio is negatively correlated with the reconstructed POC flux and the diatom-bound $\delta^{15}\text{N}$ but is positively
 400 correlated with the PIC:POC export ratio (Fig. 11c).



401 **Figure 11.** Comparison of the reconstructed POC export flux and PIC:POC ratio with previously published data for core
 402 PS75/072-4. a) Atmospheric CO₂ (black, Bereiter et al., 2015) and dust flux (brown, Lambert et al., 2012) from EPICA
 403 Dome C (EDC) ice core. b) Reconstructed deep-ocean POC flux (blue, this study) and diatom-bound $\delta^{15}\text{N}$ (black, Studer et
 404 al., 2015). c) Reconstructed PIC:POC export ratio (red, this study) and sediment Ba/Fe elemental ratio (black, Studer et al.,
 405 2015). d) Ice rafted debris (IRD) abundance from other cores in the Pacific sector : the Somov sea (McKay et al., 2022) and
 406 the Campbell plateau (Carter et al., 2002). In b) and c), the continuous line is the transfer functions average and the colored
 407 area is the transfer functions envelope. Grey and blue bars as in Fig. 6.

4.3 Consistency of the reconstructed biological and carbonate pump during glacial/interglacial periods

At the global SO scale, we report a two times higher deep-ocean POC flux during MIS 2 compared to the Holocene and a 1.5 times higher flux compared to the modern sediment trap average. This is consistent with modeling studies that quantified the difference in the upper-ocean (~100 m) POC export between the LGM and the preindustrial era in the SO : +20 % (Bopp et al., 2003), +20 % to +80 % (Tagliabue et al., 2009), +0 % to +300 % (Lambert et al., 2015), +40 % (Yamamoto et al., 2019).

Several studies previously proposed that during glacial or colder periods, export production increased in the SAZ due to iron fertilization while it decreased in the AZ due to lower nitrate supply caused by higher ocean vertical stratification (François et al., 1997; Jaccard et al., 2013; Gottschalk et al., 2016; Sigman et al., 2021). In these studies, export estimates in the SAZ are based on alkenone flux and/or $\delta^{15}\text{N}$, while in the AZ they are based on the Ba/Fe ratio or opal flux or $\delta^{15}\text{N}$ proxies. Contrasting with these findings, our study shows that the reconstructed POC export flux increases during glacial periods in the AZ, associated with high IRD inputs and high atmospheric dust flux. In core PS75/072-4, during MIS 5, the reconstructed POC flux decreases while the Ba/Fe ratio increases together with the reconstructed PIC:POC ratio (Fig. 11c). The Ba/Fe carbon export proxy is associated with several potential limitations when applied to SO sediment cores such as variations in dissolved Ba in oceanic waters and variations in barite preservation in organic matter-rich sediments (François et al., 1997; Averyt and Paytan, 2004; Hernandez-Sanchez et al., 2011). Higher PIC-export and lower organic carbon accumulation during warm periods might cause a lower sedimentary TOC content leading to a better preservation of barite in sediments, hence increasing the Ba/Fe ratio. The sensitivity of the Ba/Fe proxy to temporal changes in organic matter content and detrital or Fe inputs during glacial periods might thus explain the discrepancy between our reconstructed POC flux and the Ba/Fe elemental ratio. Indeed, a better knowledge of sediment redox conditions is needed to confirm this hypothesis.

The reconstructed POC flux increase is highly correlated with diatom-bound $\delta^{15}\text{N}$ in core PS75/072-4 (Fig. 8b) and with TOC in core PS1768-8 (Fig. 11b). Sedimentary TOC content is constrained by organic matter remineralization linked to redox conditions. Lower oxygenation of the Antarctic Bottom Water during glacial periods has been suggested from redox-sensitive trace metals, potentially leading to a better organic carbon preservation (Jaccard et al., 2016). Our results suggest that increased POC flux to the seafloor is an additional mechanism contributing to the higher TOC content during glacial periods in core PS1768-8. Diatom-bound $\delta^{15}\text{N}$ reflects the degree of nitrate utilization by phytoplankton (Altabet and Francois, 1994). During glacial periods in the AZ, high diatom-bound $\delta^{15}\text{N}$ associated with low opal accumulation rate have been interpreted as a more complete nitrate utilization caused by lower nitrate supply in the surface ocean due to higher vertical stratification, ultimately resulting in lower opal export fluxes (Studer et al., 2015). Our new transfer functions show an increase in deep-ocean POC export in the AZ during glacial periods, which could appear as inconsistent with lower opal export flux. However, an absence of correlation between TOC content and BSi content has been reported during glacial periods in sediment cores located the Indian sector of the SO (Choi et al., 2025), suggesting that opal might not be a reliable carbon export proxy. Moreover, if there is a shift from a high to low biogenic silica to POC ratio diatom community, a decrease in flux opal flux can occur (Assmy et al., 2013; Tréguer et al., 2018). A change in diatom community structure during glacial periods has been previously described in all the open-ocean sediment cores considered here (Table 2). The contribution by lightly silicified, ice-related species (factor 2) and bloom forming species (factor 3) increases to reach 20-60

% of the diatom assemblage depending on the core (Fig. S6). Concomitantly, the relative abundance of the silica-sinker *Fragilariopsis kerguelensis* decreases. Hence, the reconstructed glacial increase of POC flux associated with a decrease in opal flux could be explained by a change in the diatom community characterized by an increased contribution from carbon sinkers and a decreasing contribution by silica sinkers, together with a higher zooplankton contribution to the total POC export flux.

There are fewer estimates of the PIC:POC export ratio during the LGM. At global scale, the modeling study by Bopp et al. (2003) suggested a LGM PIC:POC export ratio 8 % lower than preindustrial, in agreement with our SO estimate of 13 % and 17 % lower MIS2 value compared to modern sediment trap data and Holocene, respectively. We found an overall good agreement between the reconstructed PIC:POC export ratio and the sediment CaCO_3 content in cores PS1768-8 and PS2606-6 which are both located above the CCD. Indeed, the sedimentary CaCO_3 content is the result of several processes including production, export and preservation of CaCO_3 in the sediment and cannot solely be interpreted in terms of PIC:POC export ratio. For example, an interglacial increase in CaCO_3 content has been attributed to the deepening of the CCD leading to a better preservation of CaCO_3 (Jaccard et al., 2013) while a glacial decrease in CaCO_3 content has been interpreted as the result of calcite dissolution due to increased primary production leading to higher organic matter remineralization (Schulte and Bard, 2003). Our results suggest that both processes (higher export and better preservation) could explain the increase in sedimentary CaCO_3 content during interglacials in the AZ.

4.4 Processes driving the biological pump and carbonate counter-pump changes in the Antarctic Zone

The global biological pump efficiency can be decomposed into two critical steps quantified by export efficiency and transfer efficiency. Export efficiency refers to the proportion of the primary production that is exported out of the mixed layer, and transfer efficiency is the fraction of exported organic matter that is not remineralized in the mesopelagic zone and reaches the deep ocean >1000 m (Henson et al., 2012; Doney et al., 2024). The analysis of the detrital fraction in sediment cores suggests that both the SAZ and the AZ were fertilized by atmospheric dust deposition during glacial periods (Struve et al., 2020). Iron fertilization could lead to the higher macronutrient utilization in the AZ deduced from increased diatom-bound $\delta^{15}\text{N}$, hence resulting in higher export efficiency mediated by bloom-forming and spore-forming diatoms (Blain et al., 2021), in agreement with the original iron hypothesis (Martin, 1990; Moore et al., 2000). Moreover, we observe a tight coupling between markers of ice presence (IRD) and increases in the reconstructed deep-ocean POC flux. The northward migration of the winter sea-ice edge during glacial periods (Crosta et al., 2022) could contribute to the increase in the large zooplankton-mediated POC export, increasing transfer efficiency. Hence, both the dust fertilization and the extended sea ice area could drive a globally more efficient biological pump during glacial periods.

The Atlantic record of core PS1768-8 shows an elevated POC flux throughout MIS 2 (Fig. 8b) whereas in the Indian and Pacific sector the POC export starts to decrease earlier, around 20 ka (Fig. 10b, 11b). This might result from two processes : different iron fertilization and/or different timing of deglaciation. Model results suggest that LGM dust fluxes were higher in the Atlantic sector, potentially leading to higher export production when compared to the other SO sectors (Lambert et al., 2015). In the Atlantic core PS1768-8, the high IRD abundance until the end of MIS 2 (Fig. 8d) suggests a longer influence of sea ice extension compared to core PS2606 in the Indian sector (Fig. 10d). Crosta et al. (2022) suggested an earlier ice retreat in the Pacific when compared to the two other sectors, although the timing of the ice retreat is not well

constrained in all the SO sectors. Reconstructions for the high temporal resolution cores PS97/72-1 and COR1GC shows that there is a substantial increase in POC export during the ACR (Fig. 6a, d). As sea ice extension notably increased during ACR (Vorrath et al., 2023), our results suggest a coupling at short time scale between changes in sea ice extension and deep-ocean POC export, supporting the idea of sea ice as an important factor driving plankton community composition and the efficiency of the biological pump (Moore et al., 2000).

A decrease in PIC content and an increase in TOC content during MIS 2 and MIS 4 was reported in multiple sediment cores located in the Indian Sector (Choi et al., 2025). These results are in agreement with our reconstructions of a lower glacial PIC:POC export ratio. The increase in the reconstructed PIC:POC ratio during deglaciations in the three sectors of the SO is tightly coupled with the decrease in IRD in SO sediments. This observation is consistent with enhanced coccolith export related to the rising sea surface temperatures and decreasing sea ice extension (Duchamp-Alphonse et al., 2018). While there is a similar higher MIS 2 POC flux in the three sector of the SO compared to the Holocene (Fig. 7a), the reconstructed MIS 2 PIC:POC export ratio in the Pacific is higher than that of the two other sectors (Fig. 7b). This geographical contrast suggests a sector-specific response of the calcifying plankton community during glacial conditions. Indeed, studies have demonstrated that coccolithophores dominates the PIC in the PFZ of the Pacific Ocean, where they are mostly represented by *Emiliania huxleyi* morphogroup B that is rare in other high latitude environments (Saavedra-Pellitero et al., 2014, 2025). Coccolithophores biogeography might be responsible for the specifically high MIS 2 PIC:POC export ratio of the Pacific sector compared to the Atlantic and the Indian sectors, although a direct quantification and identification of coccoliths in the sediment cores are necessary to confirm this hypothesis.

5 Conclusion

The compilation of sediment trap and sediment core datasets from the SO allowed us to create three new independent transfer functions to reconstruct deep-ocean POC export flux and PIC:POC ratio. The three methods (MLR, PLSR, GBR) used to design these transfer functions provide convergent results, however the PLSR and GBR approaches are associated with lower errors. The factor analysis associated with the MLR allows to identify ecologically-consistent diatom groups associated with POC export and PIC:POC ratio. High POC export is correlated with bloom-forming and resting spores-forming diatoms, as well as sea ice-related diatoms. High PIC:POC ratio is associated with warmer SAZ diatom species. Indeed, the number of sediment trap data is an inherent limitation to the precision of the transfer functions. Hence, to improve these, the sediment trap sampling effort conducted during the 1990-2010 period must be continued. Furthermore, standard deployment depth and sampling frequency coupled with a homogeneous diatom identification procedure would also increase transfer functions quality.

Based on nine sediment cores located in the three sectors of the SO, we show a POC export increase during glacial periods in the AZ. This result is in agreement with studies based on diatom-bound $\delta^{15}\text{N}$ and total organic carbon content but contradicts results based on the Ba/Fe ratio proxy. We argue that preservation of Ba in SO sediments and large temporal changes detrital and Fe inputs in this sediment core could potentially hinder the use of this latter proxy. To explain the glacial increase of POC flux observed in the AZ of the global SO, we suggest that dust-induced iron fertilization together with a northward migration of the sea ice edge during glacial periods lead to a stronger biological pump resulting from the direct export of bloom-forming diatom combined with higher export by zooplankton feeding on ice-associated diatoms. This

517 concept is consistent with the first estimate of glacial SO CO₂ sink (Moore et al., 2000) and with more recent estimates of
518 nutrient utilization in the SAZ and AZ (Wang et al., 2017). We also show that the PIC:POC ratio increases during
519 deglaciation, in agreement with the previously proposed view of a stronger carbonate counter-pump caused by the
520 concomitant development of calcifying plankton in warmer water. Our results highlight the role of SO biology in lowering
521 atmospheric CO₂ during the LGM as the result of a **twice** higher biological pump and a lower carbonate counter-pump (-17
522 %) compared to the Holocene. The application of the new proxies presented in this study to sediment cores of from the SAZ
523 could allow a direct comparison of the two SO zones, leading to a better comprehension of the latitudinal response of the
524 biological pump and carbonate counter-pump during glacial periods and at the glacial-interglacial transitions.

525 **Code and data availability**

526 The python scripts and the sediment trap and sediment core datasets are available at [https://github.com/mathieu-](https://github.com/mathieu-rembauville/so_biological_pump)
527 [rembauville/so biological pump](https://github.com/mathieu-rembauville/so_biological_pump).

528 **Authors contribution**

529 MR performed the conceptualization, data curation, formal analysis, and wrote the original manuscript. SP reviewed and
530 edited the manuscript.

531 **Competing interests**

532 The contact author has declared that none of the authors has any competing interests.

533 **Acknowledgments**

534 “We thank the two anonymous Reviewers for the constructive comments that helped us improve the manuscript.”

535 **Financial support**

536 This study was supported by CNRS INSU LEFE ‘DUST’ and ANR EXODUST (ANR-24-CE01-6090) grants to S. Pichat.

- Abelmann, A. and Gersonde, R.: Biosiliceous particle flux in the Southern Ocean, *Mar. Chem.*, 35, 503–536, [https://doi.org/10.1016/S0304-4203\(09\)90040-8](https://doi.org/10.1016/S0304-4203(09)90040-8), 1991.
- Abelmann, A., Gersonde, R., Cortese, G., Kuhn, G., and Smetacek, V.: Extensive phytoplankton blooms in the Atlantic sector of the glacial Southern Ocean, *Paleoceanography*, 21, <https://doi.org/10.1029/2005PA001199>, 2006.
- Altabet, M. A. and Francois, R.: Sedimentary nitrogen isotopic ratio as a recorder for surface ocean nitrate utilization, *Glob. Biogeochem. Cycles*, 8, 103–116, <https://doi.org/10.1029/93GB03396>, 1994.
- Anderson, H. J., Chase, Z., Bostock, H. C., Noble, T. L., Shuttleworth, R., Taiapa, B., Chen, W. H., Ren, H., and Jacobsen, G. E.: Millennial-Scale Carbon Flux Variability in the Subantarctic Pacific During Marine Isotope Stage 3 (57–29 ka), *Paleoceanogr. Paleoclimatology*, 39, e2023PA004776, <https://doi.org/10.1029/2023PA004776>, 2024.
- Anderson, R. F., Chase, Z., Fleisher, M. Q., and Sachs, J.: The Southern Ocean’s biological pump during the Last Glacial Maximum, *Deep Sea Res. Part II Top. Stud. Oceanogr.*, 49, 1909–1938, [https://doi.org/10.1016/S0967-0645\(02\)00018-8](https://doi.org/10.1016/S0967-0645(02)00018-8), 2002.
- Archer, D., Winguth, A., Lea, D., and Mahowald, N.: What caused the glacial/interglacial atmospheric pCO₂ cycles?, *Rev. Geophys.*, 38, 159–189, <https://doi.org/10.1029/1999RG000066>, 2000.
- Armand, L. K., Crosta, X., Romero, O., and Pichon, J.-J.: The biogeography of major diatom taxa in Southern Ocean sediments: 1. Sea ice related species, *Palaeogeogr. Palaeoclimatol. Palaeoecol.*, 223, 93–126, <https://doi.org/10.1016/j.palaeo.2005.02.015>, 2005.
- Assmy, P., Smetacek, V., Montresor, M., Klaas, C., Henjes, J., Strass, V. H., Arrieta, J. M., Bathmann, U., Berg, G. M., Breitbarth, E., Cisewski, B., Friedrichs, L., Fuchs, N., Herndl, G. J., Jansen, S., Kräfigsky, S., Latasa, M., Peeken, I., Röttgers, R., Scharek, R., Schüller, S. E., Steigenberger, S., Webb, A., and Wolf-Gladrow, D.: Thick-shelled, grazer-protected diatoms decouple ocean carbon and silicon cycles in the iron-limited Antarctic Circumpolar Current, *Proc. Natl. Acad. Sci. U. S. A.*, 110, 20633–20638, <https://doi.org/10.1073/pnas.1309345110>, 2013.
- Averyt, K. B. and Paytan, A.: A comparison of multiple proxies for export production in the equatorial Pacific, *Paleoceanography*, 19, <https://doi.org/10.1029/2004PA001005>, 2004.
- de Baar, H. J. W., Buma, A. G. J., Nolting, R. F., Cadée, G. C., Jacques, G., and Tréguer, P. J.: On iron limitation of the Southern Ocean: experimental observations in the Weddell and Scotia Seas, *Mar. Ecol. Prog. Ser.*, 65, 105–122, 1990.
- Belcher, A., Henson, S. A., Manno, C., Hill, S. L., Atkinson, A., Thorpe, S. E., Fretwell, P., Ireland, L., and Tarling, G. A.: Krill faecal pellets drive hidden pulses of particulate organic carbon in the marginal ice zone, *Nat. Commun.*, 10, 889, <https://doi.org/10.1038/s41467-019-08847-1>, 2019.
- Benz, V., Esper, O., Gersonde, R., Lamy, F., and Tiedemann, R.: Last Glacial Maximum sea surface temperature and sea-ice extent in the Pacific sector of the Southern Ocean, *Quat. Sci. Rev.*, 146, 216–237, <https://doi.org/10.1016/j.quascirev.2016.06.006>, 2016.

- Bereiter, B., Eggleston, S., Schmitt, J., Nehrbass-Ahles, C., Stocker, T. F., Fischer, H., Kipfstuhl, S., and Chappellaz, J.: Revision of the EPICA Dome C CO₂ record from 800 to 600 kyr before present, *Geophys. Res. Lett.*, 42, 542–549, <https://doi.org/10.1002/2014GL061957>, 2015.
- Berner, K. S., Koç, N., Divine, D., Godtliessen, F., and Moros, M.: A decadal-scale Holocene sea surface temperature record from the subpolar North Atlantic constructed using diatoms and statistics and its relation to other climate parameters, *Paleoceanography*, 23, <https://doi.org/10.1029/2006PA001339>, 2008.
- Blain, S., Rembauville, M., Crispi, O., and Obernosterer, I.: Synchronized autonomous sampling reveals coupled pulses of biomass and export of morphologically different diatoms in the Southern Ocean, *Limnol. Oceanogr.*, 66, 753–764, <https://doi.org/10.1002/lno.11638>, 2021.
- Blain, S., Planquette, H., Obernosterer, I., and Guéneuguès, A.: Vertical Flux of Trace Elements Associated With Lithogenic and Biogenic Carrier Phases in the Southern Ocean, *Glob. Biogeochem. Cycles*, 36, e2022GB007371, <https://doi.org/10.1029/2022GB007371>, 2022.
- Bopp, L., Kohfeld, K. E., Le Quéré, C., and Aumont, O.: Dust impact on marine biota and atmospheric CO₂ during glacial periods, *Paleoceanography*, 18, <https://doi.org/10.1029/2002PA000810>, 2003.
- Brandon, M., Duchamp-Alphonse, S., Michel, E., Landais, A., Isguder, G., Richard, P., Pige, N., Bassinot, F., Jaccard, S. L., and Bartolini, A.: Enhanced Carbonate Counter Pump and upwelling strengths in the Indian sector of the Southern Ocean during MIS 11, *Quat. Sci. Rev.*, 287, 107556, <https://doi.org/10.1016/j.quascirev.2022.107556>, 2022.
- Carter, L., Neil, H. L., and Northcote, L.: Late Quaternary ice-rafting events in the SW Pacific Ocean, off eastern New Zealand, *Mar. Geol.*, 191, 19–35, [https://doi.org/10.1016/S0025-3227\(02\)00509-1](https://doi.org/10.1016/S0025-3227(02)00509-1), 2002.
- Cattell, R. B.: The Scree Test For The Number Of Factors, *Multivar. Behav. Res.*, 1, 245–276, https://doi.org/10.1207/s15327906mbr0102_10, 1966.
- Choi, H., Crosta, X., Billy, I., Irino, T., Ha, S., Takata, H., and Khim, B.-K.: Orbital-scale competition of biogenic carbonate and opal production and its implication on carbon cycle at Del Caño Rise in the Indian sector of the Southern Ocean, *Palaeogeogr. Palaeoclimatol. Palaeoecol.*, 679, 113290, <https://doi.org/10.1016/j.palaeo.2025.113290>, 2025.
- Civel-Mazens, M., Crosta, X., Cortese, G., Lowe, V., Itaki, T., Ikehara, M., and Kohfeld, K.: Subantarctic jet migrations regulate vertical mixing in the Southern Indian, *Earth Planet. Sci. Lett.*, 642, 118877, <https://doi.org/10.1016/j.epsl.2024.118877>, 2024.
- Crosta, X., Pichon, J.-J., and Burckle, L. H.: Application of modern analog technique to marine Antarctic diatoms: Reconstruction of maximum sea-ice extent at the Last Glacial Maximum, *Paleoceanography*, 13, 284–297, <https://doi.org/10.1029/98PA00339>, 1998.
- Crosta, X., Kohfeld, K. E., Bostock, H. C., Chadwick, M., Du Vivier, A., Esper, O., Etourneau, J., Jones, J., Leventer, A., Müller, J., Rhodes, R. H., Allen, C. S., Ghadi, P., Lamping, N., Lange, C. B., Lawler, K.-A., Lund, D., Marzocchi, A., Meissner, K. J., Menviel, L., Nair, A., Patterson, M., Pike, J.,

- Prebble, J. G., Riesselman, C., Sadatzki, H., Sime, L. C., Shukla, S. K., Thöle, L., Vorrath, M.-E., Xiao, W., and Yang, J.: Antarctic sea ice over the past 130 000 years – Part 1: a review of what proxy records tell us, *Clim. Past*, 18, 1729–1756, <https://doi.org/10.5194/cp-18-1729-2022>, 2022.
- DeMaster, D. J., Ragueneau, O., and Nittrouer, C. A.: Preservation efficiencies and accumulation rates for biogenic silica and organic C, N, and P in high-latitude sediments: The Ross Sea, *J. Geophys. Res. Oceans*, 101, 18501–18518, <https://doi.org/10.1029/96JC01634>, 1996.
- Diekmann, B., Fütterer, D. K., Grobe, H., Hillenbrand, C.-D., Kuhn, G., Michels, K., Petschick, R., and Pirrung, M.: Ice rafted debris (> 2 mm gravel) distribution in sediment core PS1768-8, <https://doi.org/10.1594/PANGAEA.50243>, 1996.
- Doney, S. C., Mitchell, K. A., Henson, S. A., Cavan, E., DeVries, T., Gruber, N., Hauck, J., Mouw, C. B., Müller, J. D., and Primeau, F. W.: Observational and Numerical Modeling Constraints on the Global Ocean Biological Carbon Pump, *Glob. Biogeochem. Cycles*, 38, e2024GB008156, <https://doi.org/10.1029/2024GB008156>, 2024.
- Duchamp-Alphonse, S., Siani, G., Michel, E., Beaufort, L., Gally, Y., and Jaccard, S. L.: Enhanced ocean-atmosphere carbon partitioning via the carbonate counter pump during the last deglacial, *Nat. Commun.*, 9, 2396, <https://doi.org/10.1038/s41467-018-04625-7>, 2018.
- Dymond, J., Suess, E., and Lyle, M.: Barium in Deep-Sea Sediment: A Geochemical Proxy for Paleoproductivity, *Paleoceanography*, 7, 163–181, <https://doi.org/10.1029/92PA00181>, 1992.
- Esper, O. and Gersonde, R.: Quaternary surface water temperature estimations: New diatom transfer functions for the Southern Ocean, *Palaeogeogr. Palaeoclimatol. Palaeoecol.*, 414, 1–19, <https://doi.org/10.1016/j.palaeo.2014.08.008>, 2014.
- Feely, R. A., Sabine, C. L., Lee, K., Berelson, W., Kleypas, J., Fabry, V. J., and Millero, F. J.: Impact of Anthropogenic CO₂ on the CaCO₃ System in the Oceans, *Science*, 305, 362–366, <https://doi.org/10.1126/science.1097329>, 2004.
- Field, C. B., Behrenfeld, M. J., Randerson, J. T., and Falkowski, P.: Primary Production of the Biosphere: Integrating Terrestrial and Oceanic Components, *Science*, 281, 237–240, <https://doi.org/10.1126/science.281.5374.237>, 1998.
- Fischer, G., Gersonde, R., and Wefer, G.: Organic carbon, biogenic silica and diatom fluxes in the marginal winter sea-ice zone and in the Polar Front Region: interannual variations and differences in composition, *Deep Sea Res. Part II Top. Stud. Oceanogr.*, 49, 1721–1745, [https://doi.org/10.1016/S0967-0645\(02\)00009-7](https://doi.org/10.1016/S0967-0645(02)00009-7), 2002.
- François, R., Altabet, M. A., Yu, E.-F., Sigman, D. M., Bacon, M. P., Frank, M., Bohrmann, G., Bareille, G., and Labeyrie, L. D.: Contribution of Southern Ocean surface-water stratification to low atmospheric CO₂ concentrations during the last glacial period, *Nature*, 389, 929–935, <https://doi.org/10.1038/40073>, 1997.

- Francois, R., Frank, M., Rutgers van der Loeff, M. M., and Bacon, M. P.: 230Th normalization: An essential tool for interpreting sedimentary fluxes during the late Quaternary, *Paleoceanography*, 19, <https://doi.org/10.1029/2003PA000939>, 2004.
- Frankignoulle, M., Canon, C., and Gattuso, J.-P.: Marine calcification as a source of carbon dioxide: Positive feedback of increasing atmospheric CO₂, *Limnol. Oceanogr.*, 39, 458–462, <https://doi.org/10.4319/lo.1994.39.2.0458>, 1994.
- Friedman, J. H.: Greedy function approximation: A gradient boosting machine., *Ann. Stat.*, 29, 1189–1232, <https://doi.org/10.1214/aos/1013203451>, 2001.
- Gersonde, R., Crosta, X., Abelman, A., and Armand, L.: Sea-surface temperature and sea ice distribution of the Southern Ocean at the EPILOG Last Glacial Maximum—a circum-Antarctic view based on siliceous microfossil records, *Quat. Sci. Rev.*, 24, 869–896, <https://doi.org/10.1016/j.quascirev.2004.07.015>, 2005.
- Gottschalk, J., Skinner, L. C., Lippold, J., Vogel, H., Frank, N., Jaccard, S. L., and Waelbroeck, C.: Biological and physical controls in the Southern Ocean on past millennial-scale atmospheric CO₂ changes, *Nat. Commun.*, 7, 11539, <https://doi.org/10.1038/ncomms11539>, 2016.
- Grigorov, I., Rigual-Hernandez, A. S., Honjo, S., Kemp, A. E. S., and Armand, L. K.: Settling fluxes of diatoms to the interior of the Antarctic circumpolar current along 170 °W, *Deep Sea Res. Part Oceanogr. Res. Pap.*, 93, 1–13, <https://doi.org/10.1016/j.dsr.2014.07.008>, 2014.
- Grobe, H.: Sedimentology of core PS1786-1, <https://doi.org/10.1594/PANGAEA.51719>, 1996.
- Grobe, H.: Ice rafted debris (> 2 mm gravel) distribution in sediment core PS2606-6, <https://doi.org/10.1594/PANGAEA.58545>, 2001.
- Henson, S. A., Sanders, R., and Madsen, E.: Global patterns in efficiency of particulate organic carbon export and transfer to the deep ocean, *Glob. Biogeochem. Cycles*, 26, <https://doi.org/10.1029/2011GB004099>, 2012.
- Henson, S. A., Briggs, N., Carvalho, F., Manno, C., Mignot, A., and Thomalla, S.: A seasonal transition in biological carbon pump efficiency in the northern Scotia Sea, Southern Ocean, *Deep Sea Res. Part II Top. Stud. Oceanogr.*, 208, 105274, <https://doi.org/10.1016/j.dsr2.2023.105274>, 2023.
- Hernandez-Sanchez, M. T., Mills, R. A., Planquette, H., Pancost, R. D., Hepburn, L., Salter, I., and FitzGeorge-Balfour, T.: Quantifying export production in the Southern Ocean: Implications for the Baxs proxy, *Paleoceanography*, 26, <https://doi.org/10.1029/2010PA002111>, 2011.
- Honjo, S., Francois, R., Manganini, S., Dymond, J., and Collier, R.: Particle fluxes to the interior of the Southern Ocean in the Western Pacific sector along 170°W, *Deep Sea Res. Part II Top. Stud. Oceanogr.*, 47, 3521–3548, [https://doi.org/10.1016/S0967-0645\(00\)00077-1](https://doi.org/10.1016/S0967-0645(00)00077-1), 2000.
- Hutson, W. H.: The Agulhas Current During the Late Pleistocene: Analysis of Modern Faunal Analogs, *Science*, 207, 64–66, <https://doi.org/10.1126/science.207.4426.64>, 1980.

- Imbrie, J. and Kipp, N. G.: A new micropaleontological method for quantitative paleoclimatology : application to a late Pleistocene Caribbean core, *Late Cenozoic Glacial Ages*, 71–181, 1971.
- Jaccard, S. L., Hayes, C. T., Martínez-García, A., Hodell, D. A., Anderson, R. F., Sigman, D. M., and Haug, G. H.: Two Modes of Change in Southern Ocean Productivity Over the Past Million Years, *Science*, 339, 1419–1423, <https://doi.org/10.1126/science.1227545>, 2013.
- Jaccard, S. L., Galbraith, E. D., Martínez-García, A., and Anderson, R. F.: Covariation of deep Southern Ocean oxygenation and atmospheric CO₂ through the last ice age, *Nature*, 530, 207–210, <https://doi.org/10.1038/nature16514>, 2016.
- Jackson, D. A.: Stopping Rules in Principal Components Analysis: A Comparison of Heuristical and Statistical Approaches, *Ecology*, 74, 2204–2214, <https://doi.org/10.2307/1939574>, 1993.
- Jacot Des Combes, H., Esper, O., De La Rocha, C. L., Abelmann, A., Gersonde, R., Yam, R., and Shemesh, A.: Diatom $\delta^{13}\text{C}$, $\delta^{15}\text{N}$, and C/N since the Last Glacial Maximum in the Southern Ocean: Potential impact of Species Composition, *Paleoceanography*, 23, <https://doi.org/10.1029/2008PA001589>, 2008.
- Jin, X., Gruber, N., Dunne, J. P., Sarmiento, J. L., and Armstrong, R. A.: Diagnosing the contribution of phytoplankton functional groups to the production and export of particulate organic carbon, CaCO₃, and opal from global nutrient and alkalinity distributions, *Glob. Biogeochem. Cycles*, 20, <https://doi.org/10.1029/2005GB002532>, 2006.
- Juggins, S.: Quantitative reconstructions in palaeolimnology: new paradigm or sick science?, *Quat. Sci. Rev.*, 64, 20–32, <https://doi.org/10.1016/j.quascirev.2012.12.014>, 2013.
- Kohfeld, K. E., Quéré, C. L., Harrison, S. P., and Anderson, R. F.: Role of Marine Biology in Glacial-Interglacial CO₂ Cycles, *Science*, 308, 74–78, <https://doi.org/10.1126/science.1105375>, 2005.
- Kuhn, G.: Sedimentology of core PS1786-1, <https://doi.org/10.1594/PANGAEA.51132>, 1996.
- Kuhn, G.: Calcium carbonate content of sediment core PS2606-6, <https://doi.org/10.1594/PANGAEA.93723>, 2003.
- Kuhn, G. and Bohrmann, G.: Sedimentology of core PS1768-8, <https://doi.org/10.1594/PANGAEA.51126>, 1996.
- Lambert, F., Bigler, M., Steffensen, J. P., Hutterli, M., and Fischer, H.: Centennial mineral dust variability in high-resolution ice core data from Dome C, Antarctica, *Clim. Past*, 8, 609–623, <https://doi.org/10.5194/cp-8-609-2012>, 2012.
- Lambert, F., Tagliabue, A., Shaffer, G., Lamy, F., Winckler, G., Farias, L., Gallardo, L., and De Pol-Holz, R.: Dust fluxes and iron fertilization in Holocene and Last Glacial Maximum climates, *Geophys. Res. Lett.*, 42, 6014–6023, <https://doi.org/10.1002/2015GL064250>, 2015.
- Leventer, A.: Sediment trap diatom assemblages from the northern Antarctic Peninsula region, *Deep Sea Res. Part Oceanogr. Res. Pap.*, 38, 1127–1143, [https://doi.org/10.1016/0198-0149\(91\)90099-2](https://doi.org/10.1016/0198-0149(91)90099-2), 1991.

- Maloney, K. O., Schmid, M., and Weller, D. E.: Applying additive modelling and gradient boosting to assess the effects of watershed and reach characteristics on riverine assemblages, *Methods Ecol. Evol.*, 3, 116–128, <https://doi.org/10.1111/j.2041-210X.2011.00124.x>, 2012.
- Manno, C., Stowasser, G., Enderlein, P., Fielding, S., and Tarling, G. A.: The contribution of zooplankton faecal pellets to deep-carbon transport in the Scotia Sea (Southern Ocean), *Biogeosciences*, 12, 1955–1965, <https://doi.org/10.5194/bg-12-1955-2015>, 2015.
- Manno, C., Stowasser, G., Fielding, S., Apeland, B., and Tarling, G. A.: Deep carbon export peaks are driven by different biological pathways during the extended Scotia Sea (Southern Ocean) bloom, *Deep Sea Res. Part II Top. Stud. Oceanogr.*, 205, 105183, <https://doi.org/10.1016/j.dsr2.2022.105183>, 2022.
- Marsay, C. M., Sanders, R. J., Henson, S. A., Pabortsava, K., Achterberg, E. P., and Lampitt, R. S.: Attenuation of sinking particulate organic carbon flux through the mesopelagic ocean, *Proc. Natl. Acad. Sci.*, 112, 1089–1094, <https://doi.org/10.1073/pnas.1415311112>, 2015.
- Martin, J. H.: Glacial-interglacial CO₂ change: The Iron Hypothesis, *Paleoceanography*, 5, 1–13, <https://doi.org/10.1029/PA005i001p00001>, 1990.
- Martin, J. H., Knauer, G. A., Karl, D. M., and Broenkow, W. W.: VERTEX: carbon cycling in the northeast Pacific, *Deep Sea Res. Part Oceanogr. Res. Pap.*, 34, 267–285, [https://doi.org/10.1016/0198-0149\(87\)90086-0](https://doi.org/10.1016/0198-0149(87)90086-0), 1987.
- Martínez-García, A., Sigman, D. M., Ren, H., Anderson, R. F., Straub, M., Hodell, D. A., Jaccard, S. L., Eglinton, T. I., and Haug, G. H.: Iron Fertilization of the Subantarctic Ocean During the Last Ice Age, *Science*, 343, 1347–1350, <https://doi.org/10.1126/science.1246848>, 2014.
- McKay, R., Albot, O., Dunbar, G. B., Lee, J. I., Lee, M. K., Yoo, K.-C., Kim, S., Turton, N., Kulhanek, D., Patterson, M., and Levy, R.: A Comparison of Methods for Identifying and Quantifying Ice Rafted Debris on the Antarctic Margin, *Paleoceanogr. Paleoclimatology*, 37, e2021PA004404, <https://doi.org/10.1029/2021PA004404>, 2022.
- Moore, J. K., Abbott, M. R., Richman, J. G., and Nelson, D. M.: The southern ocean at the Last Glacial Maximum: A strong sink for atmospheric carbon dioxide, *Glob. Biogeochem. Cycles*, 14, 455–475, <https://doi.org/10.1029/1999GB900051>, 2000.
- O’Brien, C., Virtue, P., Kawaguchi, S., and Nichols, P. D.: Aspects of krill growth and condition during late winter-early spring off East Antarctica (110–130°E), *Deep Sea Res. Part II Top. Stud. Oceanogr.*, 58, 1211–1221, <https://doi.org/10.1016/j.dsr2.2010.11.001>, 2011.
- Oetjens, A., Chase, Z., Strutton, P., and Rohr, T.: An improved model of particle attenuation reduces estimates of Southern Ocean carbon transfer efficiency, *Commun. Earth Environ.*, 6, 1041, <https://doi.org/10.1038/s43247-025-03090-7>, 2025.
- Orme, L. C., Crosta, X., Miettinen, A., Divine, D. V., Husum, K., Isaksson, E., Wacker, L., Mohan, R., Ther, O., and Ikehara, M.: Sea surface temperature in the Indian sector of the Southern Ocean over the Late Glacial and Holocene, *Clim. Past*, 16, 1451–1467, <https://doi.org/10.5194/cp-16-1451-2020>, 2020.

- Pauli, N.-C., Metfies, K., Pakhomov, E. A., Neuhaus, S., Graeve, M., Wenta, P., Flintrop, C. M., Badewien, T. H., Iversen, M. H., and Meyer, B.: Selective feeding in Southern Ocean key grazers—diet composition of krill and salps, *Commun. Biol.*, 4, 1061, <https://doi.org/10.1038/s42003-021-02581-5>, 2021.
- Pedregosa, F., Varoquaux, G., Gramfort, A., Michel, V., Thirion, B., Grisel, O., Blondel, M., Prettenhofer, P., Weiss, R., Dubourg, V., Vanderplas, J., Passos, A., Cournapeau, D., Brucher, M., Perrot, M., and Duchesnay, É.: Scikit-learn: Machine Learning in Python, *J. Mach. Learn. Res.*, 12, 2825–2830, 2011.
- Pellegrino, L., Natalicchio, M., Cotellucci, A., Genre, A., Jordan, R. W., Carnevale, G., and Dela Pierre, F.: The Impact of Early Diagenesis on Biosignature Preservation in Sulfate Evaporites: Insights From Messinian (Late Miocene) Gypsum, *Geobiology*, 22, e70007, <https://doi.org/10.1111/gbi.70007>, 2024.
- Pesjak, L., McMinn, A., Chase, Z., and Bostock, H.: Sea ice and productivity changes over the last glacial cycle in the Adélie Land region, East Antarctica, based on diatom assemblage variability, *Clim. Past*, 19, 419–437, <https://doi.org/10.5194/cp-19-419-2023>, 2023.
- Petit, J. R., Jouzel, J., Raynaud, D., Barkov, N. I., Barnola, J.-M., Basile, I., Bender, M., Chappellaz, J., Davis, M., Delaygue, G., Delmotte, M., Kotlyakov, V. M., Legrand, M., Lipenkov, V. Y., Lorius, C., PÉpin, L., Ritz, C., Saltzman, E., and Stievenard, M.: Climate and atmospheric history of the past 420,000 years from the Vostok ice core, Antarctica, *Nature*, 399, 429–436, <https://doi.org/10.1038/20859>, 1999.
- Pudsey, C. J. and King, P.: Particle fluxes, benthic processes and the palaeoenvironmental record in the Northern Weddell Sea, *Deep Sea Res. Part Oceanogr. Res. Pap.*, 44, 1841–1876, [https://doi.org/10.1016/S0967-0637\(97\)00064-2](https://doi.org/10.1016/S0967-0637(97)00064-2), 1997.
- Ran, L., Wiesner, M. G., Liang, Y., Liang, W., Zhang, L., Yang, Z., Li, H., and Chen, J.: Differential dissolution of biogenic silica significantly affects the utility of sediment diatoms as paleoceanographic proxies, *Limnol. Oceanogr.*, 69, 467–481, <https://doi.org/10.1002/lno.12492>, 2024.
- Rembauville, M., Blain, S., Armand, L., Quéguiner, B., and Salter, I.: Export fluxes in a naturally iron-fertilized area of the Southern Ocean – Part 2: Importance of diatom resting spores and faecal pellets for export, *Biogeosciences*, 12, 3171–3195, <https://doi.org/10.5194/bg-12-3171-2015>, 2015.
- Rembauville, M., Meilland, J., Ziveri, P., Schiebel, R., Blain, S., and Salter, I.: Planktic foraminifer and coccolith contribution to carbonate export fluxes over the central Kerguelen Plateau, *Deep Sea Res. Part Oceanogr. Res. Pap.*, 111, 91–101, <https://doi.org/10.1016/j.dsr.2016.02.017>, 2016a.
- Rembauville, M., Manno, C., Tarling, G. A., Blain, S., and Salter, I.: Strong contribution of diatom resting spores to deep-sea carbon transfer in naturally iron-fertilized waters downstream of South Georgia, *Deep Sea Res. Part Oceanogr. Res. Pap.*, 115, 22–35, <https://doi.org/10.1016/j.dsr.2016.05.002>, 2016b.
- Rembauville, M., Briggs, N., Ardyna, M., Uitz, J., Catala, P., Penkerch, C., Poteau, A., Claustre, H., and Blain, S.: Plankton Assemblage Estimated with BGC-Argo Floats in the Southern Ocean:

- Implications for Seasonal Successions and Particle Export, *J. Geophys. Res. Oceans*, 122, 8278–8292, <https://doi.org/10.1002/2017JC013067>, 2017.
- Rigual-Hernández, A. S., Trull, T. W., Bray, S. G., Cortina, A., and Armand, L. K.: Latitudinal and temporal distributions of diatom populations in the pelagic waters of the Subantarctic and Polar Frontal zones of the Southern Ocean and their role in the biological pump, *Biogeosciences*, 12, 5309–5337, <https://doi.org/10.5194/bg-12-5309-2015>, 2015a.
- Rigual-Hernández, A. S., Trull, T. W., Bray, S. G., Closset, I., and Armand, L. K.: Seasonal dynamics in diatom and particulate export fluxes to the deep sea in the Australian sector of the southern Antarctic Zone, *J. Mar. Syst.*, 142, 62–74, <https://doi.org/10.1016/j.jmarsys.2014.10.002>, 2015b.
- Rigual-Hernández, A. S., Trull, T. W., Bray, S. G., and Armand, L. K.: The fate of diatom valves in the Subantarctic and Polar Frontal Zones of the Southern Ocean: Sediment trap versus surface sediment assemblages, *Palaeogeogr. Palaeoclimatol. Palaeoecol.*, 457, 129–143, <https://doi.org/10.1016/j.palaeo.2016.06.004>, 2016.
- Rigual-Hernández, A. S., Pilskałn, C. H., Cortina, A., Abrantes, F., and Armand, L. K.: Diatom species fluxes in the seasonally ice-covered Antarctic Zone: New data from offshore Prydz Bay and comparison with other regions from the eastern Antarctic and western Pacific sectors of the Southern Ocean, *Deep Sea Res. Part II Top. Stud. Oceanogr.*, 161, 92–104, <https://doi.org/10.1016/j.dsr2.2018.06.005>, 2019.
- Saavedra-Pellitero, M., Baumann, K.-H., Flores, J.-A., and Gersonde, R.: Biogeographic distribution of living coccolithophores in the Pacific sector of the Southern Ocean, *Mar. Micropaleontol.*, 109, 1–20, <https://doi.org/10.1016/j.marmicro.2014.03.003>, 2014.
- Saavedra-Pellitero, M., Baumann, K.-H., Bachiller-Jareno, N., Lovell, H., Vollmar, N. M., and Malinverno, E.: Mismatch between coccolithophore-based estimates of particulate inorganic carbon (PIC) concentration and satellite-derived PIC concentration in the Pacific Southern Ocean, *Biogeosciences*, 22, 3143–3164, <https://doi.org/10.5194/bg-22-3143-2025>, 2025.
- Salter, I.: Seasonal variability in the persistence of dissolved environmental DNA (eDNA) in a marine system: The role of microbial nutrient limitation, *PLOS ONE*, 13, e0192409, <https://doi.org/10.1371/journal.pone.0192409>, 2018.
- Salter, I., Kemp, A. E. S., Moore, C. M., Lampitt, R. S., Wolff, G. A., and Holtvoeth, J.: Diatom resting spore ecology drives enhanced carbon export from a naturally iron-fertilized bloom in the Southern Ocean, *Glob. Biogeochem. Cycles*, 26, <https://doi.org/10.1029/2010GB003977>, 2012.
- Salter, I., Schiebel, R., Ziveri, P., Movellan, A., Lampitt, R., and Wolff, G. A.: Carbonate counter pump stimulated by natural iron fertilization in the Polar Frontal Zone, *Nat. Geosci.*, 7, 885–889, <https://doi.org/10.1038/geo2285>, 2014.
- Sarmiento, J. L. and Toggweiler, J. R.: A new model for the role of the oceans in determining atmospheric P CO₂, *Nature*, 308, 621–624, <https://doi.org/10.1038/308621a0>, 1984.

- Sarmiento, J. L., Dunne, J., Gnanadesikan, A., Key, R. M., Matsumoto, K., and Slater, R.: A new estimate of the CaCO₃ to organic carbon export ratio, *Glob. Biogeochem. Cycles*, 16, 54-1-54-12, <https://doi.org/10.1029/2002GB001919>, 2002.
- Sarmiento, J. L., Gruber, N., Brzezinski, M. A., and Dunne, J. P.: High-latitude controls of thermocline nutrients and low latitude biological productivity, *Nature*, 427, 56–60, <https://doi.org/10.1038/nature02127>, 2004.
- Schmidt, K., Atkinson, A., Pond, D. W., and Ireland, L. C.: Feeding and overwintering of Antarctic krill across its major habitats: The role of sea ice cover, water depth, and phytoplankton abundance, *Limnol. Oceanogr.*, 59, 17–36, <https://doi.org/10.4319/lo.2014.59.1.0017>, 2014.
- Schulte, S. and Bard, E.: Past changes in biologically mediated dissolution of calcite above the chemical lysocline recorded in Indian Ocean sediments, *Quat. Sci. Rev.*, 22, 1757–1770, [https://doi.org/10.1016/S0277-3791\(03\)00172-0](https://doi.org/10.1016/S0277-3791(03)00172-0), 2003.
- Shoenfelt, E. M., Winckler, G., Lamy, F., Anderson, R. F., and Bostick, B. C.: Highly bioavailable dust-borne iron delivered to the Southern Ocean during glacial periods, *Proc. Natl. Acad. Sci.*, 115, 11180–11185, <https://doi.org/10.1073/pnas.1809755115>, 2018.
- Siegel, D. A., DeVries, T., Doney, S. C., and Bell, T.: Assessing the sequestration time scales of some ocean-based carbon dioxide reduction strategies, *Environ. Res. Lett.*, 16, 104003, <https://doi.org/10.1088/1748-9326/ac0be0>, 2021.
- Sigman, D. M., Hain, M. P., and Haug, G. H.: The polar ocean and glacial cycles in atmospheric CO₂ concentration, *Nature*, 466, 47–55, <https://doi.org/10.1038/nature09149>, 2010.
- Sigman, D. M., Fripiat, F., Studer, A. S., Kemeny, P. C., Martínez-García, A., Hain, M. P., Ai, X., Wang, X., Ren, H., and Haug, G. H.: The Southern Ocean during the ice ages: A review of the Antarctic surface isolation hypothesis, with comparison to the North Pacific, *Quat. Sci. Rev.*, 254, 106732, <https://doi.org/10.1016/j.quascirev.2020.106732>, 2021.
- Smith, A. J. R., Wotherspoon, S., Ratnarajah, L., Cutter, G. R., Macaulay, G. J., Hutton, B., King, R., Kawaguchi, S., and Cox, M. J.: Antarctic krill vertical migrations modulate seasonal carbon export, *Science*, 387, eadq5564, <https://doi.org/10.1126/science.adq5564>, 2025.
- Stein, K., Timmermann, A., Kwon, E. Y., and Friedrich, T.: Timing and magnitude of Southern Ocean sea ice/carbon cycle feedbacks, *Proc. Natl. Acad. Sci.*, 117, 4498–4504, <https://doi.org/10.1073/pnas.1908670117>, 2020.
- Stephens, B. B. and Keeling, R. F.: The influence of Antarctic sea ice on glacial–interglacial CO₂ variations, *Nature*, 404, 171–174, <https://doi.org/10.1038/35004556>, 2000.
- Struve, T., Pahnke, K., Lamy, F., Wengler, M., Böning, P., and Winckler, G.: A circumpolar dust conveyor in the glacial Southern Ocean, *Nat. Commun.*, 11, 5655, <https://doi.org/10.1038/s41467-020-18858-y>, 2020.

- Studer, A. S., Sigman, D. M., Martínez-García, A., Benz, V., Winckler, G., Kuhn, G., Esper, O., Lamy, F., Jaccard, S. L., Wacker, L., Oleynik, S., Gersonde, R., and Haug, G. H.: Antarctic Zone nutrient conditions during the last two glacial cycles, *Paleoceanography*, 30, 845–862, <https://doi.org/10.1002/2014PA002745>, 2015.
- Studer, A. S., Sigman, D. M., Martínez-García, A., Thöle, L. M., Michel, E., Jaccard, S. L., Lippold, J. A., Mazaud, A., Wang, X. T., Robinson, L. F., Adkins, J. F., and Haug, G. H.: Increased nutrient supply to the Southern Ocean during the Holocene and its implications for the pre-industrial atmospheric CO₂ rise, *Nat. Geosci.*, 11, 756–760, <https://doi.org/10.1038/s41561-018-0191-8>, 2018.
- Tagliabue, A., Bopp, L., Roche, D. M., Bouttes, N., Dutay, J.-C., Alkama, R., Kageyama, M., Michel, E., and Paillard, D.: Quantifying the roles of ocean circulation and biogeochemistry in governing ocean carbon-13 and atmospheric carbon dioxide at the last glacial maximum, *Clim. Past*, 5, 695–706, <https://doi.org/10.5194/cp-5-695-2009>, 2009.
- Thöle, L. M., Amsler, H. E., Moretti, S., Auderset, A., Gilgannon, J., Lippold, J., Vogel, H., Crosta, X., Mazaud, A., Michel, E., Martínez-García, A., and Jaccard, S. L.: Glacial-interglacial dust and export production records from the Southern Indian Ocean, *Earth Planet. Sci. Lett.*, 525, 115716, <https://doi.org/10.1016/j.epsl.2019.115716>, 2019.
- Toggweiler, J. R.: Variation of atmospheric CO₂ by ventilation of the ocean’s deepest water, *Paleoceanography*, 14, 571–588, <https://doi.org/10.1029/1999PA900033>, 1999.
- Tréguer, P., Bowler, C., Moriceau, B., Dutkiewicz, S., Gehlen, M., Aumont, O., Bittner, L., Dugdale, R., Finkel, Z., Iudicone, D., Jahn, O., Guidi, L., Lasbleiz, M., Leblanc, K., Levy, M., and Pondaven, P.: Influence of diatom diversity on the ocean biological carbon pump, *Nat. Geosci.*, 11, 27–37, <https://doi.org/10.1038/s41561-017-0028-x>, 2018.
- Uitz, J., Claustre, H., Gentili, B., and Stramski, D.: Phytoplankton class-specific primary production in the world’s oceans: Seasonal and interannual variability from satellite observations, *Glob. Biogeochem. Cycles*, 24, <https://doi.org/10.1029/2009GB003680>, 2010.
- Vollmer, T. D., Ito, T., and Lynch-Stieglitz, J.: Proxy-Based Preformed Phosphate Estimates Point to Increased Biological Pump Efficiency as Primary Cause of Last Glacial Maximum CO₂ Drawdown, *Paleoceanogr. Paleoclimatology*, 37, e2021PA004339, <https://doi.org/10.1029/2021PA004339>, 2022.
- Vorrath, M.-E., Müller, J., Cárdenas, P., Opel, T., Mieruch, S., Esper, O., Lembke-Jene, L., Etourneau, J., Vieth-Hillebrand, A., Lahajnar, N., Lange, C. B., Leventer, A., Evangelinos, D., Escutia, C., and Mollenhauer, G.: Deglacial and Holocene sea-ice and climate dynamics in the Bransfield Strait, northern Antarctic Peninsula, *Clim. Past*, 19, 1061–1079, <https://doi.org/10.5194/cp-19-1061-2023>, 2023.
- Waelbroeck, C., Paul, A., Kucera, M., Rosell-Melé, A., Weinelt, M., Schneider, R., Mix, A. C., Abelmann, A., Armand, L., Bard, E., Barker, S., Barrows, T. T., Benway, H., Cacho, I., Chen, M.-T., Cortijo, E., Crosta, X., de Vernal, A., Dokken, T., Duprat, J., Elderfield, H., Eynaud, F., Gersonde, R., Hayes, A., Henry, M., Hillaire-Marcel, C., Huang, C.-C., Jansen, E., Juggins, S., Kallel, N., Kiefer, T., Kienast, M., Labeyrie, L., Leclaire, H., Londeix, L., Mangin, S., Matthiessen, J., Marret, F., Meland, M., Morey, A. E., Mulitza, S., Pflaumann, U., Pisias, N. G., Radi, T., Rochon, A., Rohling, E. J., Saffi, S.,

- L., Schäfer-Neth, C., Solignac, S., Spero, H., Tachikawa, K., Turon, J.-L., and MARGO Project Members: Constraints on the magnitude and patterns of ocean cooling at the Last Glacial Maximum, *Nat. Geosci.*, 2, 127–132, <https://doi.org/10.1038/ngeo411>, 2009.
- Wang, X. T., Sigman, D. M., Prokopenko, M. G., Adkins, J. F., Robinson, L. F., Hines, S. K., Chai, J., Studer, A. S., Martínez-García, A., Chen, T., and Haug, G. H.: Deep-sea coral evidence for lower Southern Ocean surface nitrate concentrations during the last ice age, *Proc. Natl. Acad. Sci.*, 114, 3352–3357, <https://doi.org/10.1073/pnas.1615718114>, 2017.
- Warnock, J. P. and Krueger, R. E.: A record of diatom preservation from the AND-1B drillcore: The significance of taphofacies on diatom preservation, *Mar. Micropaleontol.*, 158, 101887, <https://doi.org/10.1016/j.marmicro.2020.101887>, 2020.
- Williams, J. R., Giering, S. L. C., Baker, C. A., Pabortsava, K., Briggs, N., East, H., Espinola, B., Blackbird, S., Le Moigne, F. a. C., Villa-Alfageme, M., Poulton, A. J., Carvalho, F., Pebody, C., Saw, K., Moore, C. M., Henson, S. A., Sanders, R., and Martin, A. P.: Inefficient transfer of diatoms through the subpolar Southern Ocean twilight zone, *Nat. Geosci.*, 18, 72–77, <https://doi.org/10.1038/s41561-024-01602-2>, 2025.
- Yamamoto, A., Abe-Ouchi, A., Ohgaito, R., Ito, A., and Oka, A.: Glacial CO₂ decrease and deep-water deoxygenation by iron fertilization from glaciogenic dust, *Clim. Past*, 15, 981–996, <https://doi.org/10.5194/cp-15-981-2019>, 2019.
- Zúñiga, D., Sanchez-Vidal, A., Flexas, M. M., Carroll, D., Rufino, M. M., Spreen, G., Calafat, A., and Abrantes, F.: Sinking Diatom Assemblages as a Key Driver for Deep Carbon and Silicon Export in the Scotia Sea (Southern Ocean), *Front. Earth Sci.*, 9, <https://doi.org/10.3389/feart.2021.579198>, 2021.